Department of Precision and Microsystems Engineering

Engineering and tuning GHz SAWs in suspended SiN membranes

András Soltész

Report no : 2024.044
Coaches : Dr. R.A. Norte and Dr. G.J. Verbiest
Type of report : Master Thesis
Date : 19-June-2024

Delft University of Technology

MSc Thesis

Department of Precision and Microsystems Engineering

Engineering and tuning GHz SAWs in suspended SiN membranes

Author
András Soltész

Supervisors
Dr. R.A. Norte
Dr. G.J. Verbiest

Mentor
R.H. Guis, MSc

June 19, 2024

Acknowledgments

I would like to express my deep gratitude to R.H. Guis, MSc, who has lent me his laser measurement setup and supported me during my experiments and research. I would also like to deeply thank Dr. R.A. Norte and Dr. G.J. Verbiest for supervising and steering my work, and meeting me regularly to discuss the progress of the project. Furthermore, my gratitude goes out for Dr. M. Khokhar and L. Norder, MSc for preparing and manufacturing my samples, and for M. Xu, MSc for providing suspended SiN membranes for my experiments.

Abstract

This thesis investigates the generation, guiding and tunability of GHz Surface Acoustic Waves (SAWs) on suspended silicon-nitride (Si3N4) membranes using a femtosecond laser pump-probe setup. A primary focus is on demonstrating an alternative photoacoustic method for tuning SAWs on the sample with a femtosecond laser. Experimental results highlight the setup's capability to excite and detect acoustic waves across suspended SiN membranes and the tunability of SAWs with the fs laser setup in the 0.1-0.3 GHz range. Furthermore, the report presents designs of acoustic waveguides and beam splitters for the guiding and splitting of selected acoustic modes, thereby contributing to the growing research in the field of Phononic Integrated Circuits (PnICs). Qualitative measurements demonstrate the successful guiding and splitting of acoustic 0.1 GHz waves on the designed suspended SiN PnC waveguides.

Contents

1 Introduction

Photonic and electric circuits serve humanity in countless ways. They are cornerstones of the technological capabilities of today's world by allowing for fast computation and communication, but also for sensing applications. However, electromagnetic radiation and electricity are not the only physical phenomena that can serve the above mentioned purposes: acoustic waves can do that too. Surface Acoustic wave (SAW) devices are already being used and developed in the field of sensing[1], telecommunication/signal processing [2] in the form of frequency filters[3], and delay lines [4], and more. Moreover, recent SAW devices have promising potential for application in the quantum regime[5], for example in single particle manipulation[6]. SAW devices can be ultracompact, as the wavelength of acoustic waves are 5 orders of magnitude smaller compared to electromagnetic waves, making them excellent candidates for GHz on-chip applications.[7]
Due to the above mentioned wide range of possible applications and the ever growing capabilities of manufacturing micro and nanoscale devices, more and more research is going into how to excite, guide, sense and route acoustic waves as efficiently as possible in on-chip applications. Such devices are often referred to as Phononic Integrated Circuits, or PnIC's. One building block of a PnIC is an acoustic or phononic waveguide. Such on-chip waveguides are widely researched [8][9][10][11]. These waveguides can be made of different materials and structures. Examples of which are: suspended membranes[10], suspended phononic crystals with line defects[12] or unreleased layered circuits[13][14].
Suspended waveguides usually make use of so called Phononic Crystal structures (PnC) to efficiently guide an acoustic wave. Much like photonic crystals, PnCs also have bandgaps: a range of frequencies of an acoustic wave or phonon that can not propagate within the structure. This property makes PnCs good isolators of acoustic waves.
Another building block of PnICs is the splitting of acoustic beams in a controlled fashion. Just as splitting light with a beam splitter enhances the capabilities of photonics, splitting of the traveling acoustic waves opens the door for new applications. As an example, one could build an "acoustic interferometer". Similar to a laser interferometer, where a coherent acoustic beam is split in two separate arms and then recombined. The change in interference of the combined signal is then the output of the sensor. Because of the small wavelength of acoustic waves at GHz frequencies, such a device could be very sensitive and compact.

There are instances of unreleased acoustic beam splitters[13][14]. However, no examples of suspended acoustic beam splitters have been found in literature.[15].
This created a knowledge gap in PnC based suspended beam splitters that was presented and addressed by M. van der Vis[15] who designed and simulated such a device. In his Master Thesis work he introduces a high-stress Si3N4 acoustic beam splitter. Simulations show it could behave as a waveguide for GHz acoustic waves and successfully split incoming acoustic beams in two separate directions. In my work presented in this report I build upon these simulations by optimizing and validating them, and finally by using them to design several suspended PnC based acoustic waveguides and splitters. These devices are then manufactured for testing.

To be able to test such a device, very sensitive measurement equipment is needed that can detect picometer surface displacements. A femtosecond laser pump-probe reflectometry/BDD setup has been made available for the project, developed by M. Robin and R. Guis et al. at TU Delft[16]. Such a setup uses strong laser pulses to heat the sample surface periodically (pump pulse), causing periodic mechanical strain that result in acoustic waves due to thermal expansion in the sample. Another, weaker laser pulse (probe pulse) is focused and reflected back from the sample to a detector to measure the change in the reflected light intensity. Changes in this intensity can then be correlated to the acoustic waves present on the material surface. The setup used in this project was developed to detect Bulk Acoustic Waves and was never applied to SAWs. It therefore raised further questions on how and if this laser pump-probe setup is capable to test a PnC based acoustic waveguide and beam splitter by exciting and probing SAWs on it at different locations.

When using (PnC based) waveguides, it is important to be able to determine (i.e. tune) the frequency of the SAW it is exciting. Tunability is important for the verification of the bandgap of the PnC, and for the excitation of acoustic waves on the waveguide that fall within this bandgap. This can be achieved by creating periodic strain patterns on the sample surface. The distance of a period determines the wavelength of the SAW. In reflectometry pulse laser pump-probe setups this has been achieved either by manufacturing periodic metal bars on the sample surface to then simply excite the bars with the pump laser spot, or by creating periodic interference patterns of the pump laser on the surface. In literature, the tunable interference pattern method has not yet been applied in combination with a femtosecond reflectivity laser setup. A challenge lies in the femtosecond laser having an extremely short laser pulse. This short laser pulse makes it challenging to implement the existing SAW tunability methods found in literature.

Thesis project objectives:

The main objective of this thesis project is to work towards the realization of a suspended GHz acoustic SiN beam splitter. This is done by first addressing the following research questions regarding the ultrafast fs pump-probe laser setup used to test such devices:

1. How to generate tunable SAWs with a reflectometry/BDD femtosecond pump-probe laser setup?
2. Is the reflectometry/BDD femtosecond pump-probe laser setup capable of exciting and detecting SAWs on a suspended SiN membrane, even at longer distances?

In this report the method and results to these questions are outlined and discussed. A new design is presented that allows the easy conversion of a reflectometry pump-probe setup to excite tunable SAWs on a sample. Experimental results of GHz acoustic waves being excited and detected on a suspended SiN membrane, even at larger distances, are presented and discussed. Furthermore, optimized designs of suspended acoustic waveguides and splitters are manufactured and qualitative tests are conducted that demonstrate the guiding and splitting of 0.1 GHz acoustic waves.

2 Technical Background

This section provides technical background on suspended phononic crystals and acoustic waveguides. It present the motivation for designing and manufacturing an acoustic beam splitter. State of the Art literature is presented on the tunable excitation and detection laser pump-probe techniques of GHz SAWs.

2.1 Suspended Phononic Crystals and Acoustic Waveguides

Suspended Phononic Crystals (PnCs) are increasingly researched for their capabilities of guiding acoustic waves.[9][10][11][17][18]. These structures are engineered meta-materials with periodic inclusions, as shown in Figure 1a. These patterned inclusions behave as scatterers for certain acoustic frequencies[19], in certain, or all directions within the crystal lattice. This means that these frequencies are "blocked" by the crystal, i.e they can not propagate in it. The range of such frequencies are the so called bandgaps of a phononic crystal. For a specific PnC they can be found by determining the band diagram of the PnC, which shows how vibrational modes of the crystal structure vary with the wave vector. See Figure 1b for an example of a band diagram, with a bandgap at 3.40 GHz.

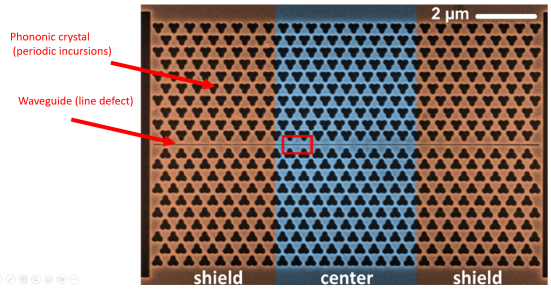

(a) Top view of a phononic crystal introducied by Madiot et. al[9]. The periodic arrangement of the holes in the membrane greatly reduce the dissipation of phonon/acoustic waves with certain frequencies.

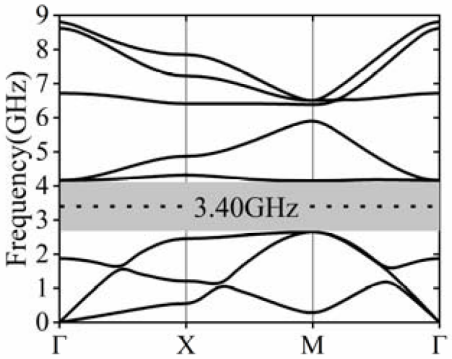

(b) Typical band diagram of a circular shaped phononic crystal presented by Zhang et al. [20]. A full bandgap in this example is around 3.40 GHz, as no vibrational modes (black lines) enter that area for any direction within the crystal lattice (x axis).

Figure 1: Examples of a phononic crystal and a band diagram

Tuning the shape, the size and the spacial periodicity of the incursions of the PnC allow for the design of the bandgaps.. As shown in Figure 2, several types of phononic crystal lattice patterns can be created, each pattern resulting in unique band diagrams.

If then a "line defect" is added to the structure that disrupts the periodicity of the crystal (see Figure 1a), the line defect can serve as an acoustic waveguide for some acoustic modes. When an acoustic frequency is excited within this waveguide (line defect) that falls in the bandgap of the PnC, the acoustic wave can not propagate within the PnC and so it will be confined to the waveguide.

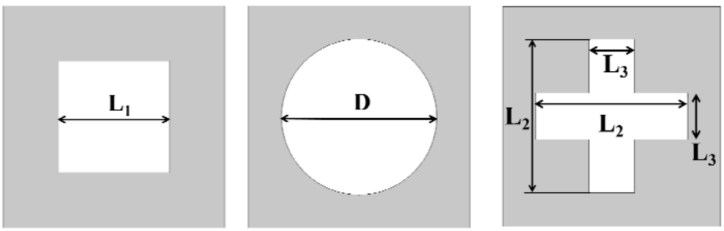

Figure 2: Different phononic crystal lattice patterns studied by Zhang et al. [20]. L1, D, L2 and L3 are design parameters that allow tuning the phononic crystal for its bandgap.

2.2 Project Background: Design of a GHz acoustic beam splitter for room temperature operation

In his Master Thesis, M. van der Vis[15] presents a design of a novel suspended SiN GHz acoustic beam splitter, see Figure 3. This design preceded an extensive literature research of suspended acoustic waveguides, claiming the novelty of such an acoustic beam splitter. Simulations were made of the design, but it has not yet been fabricated and tested. It consists of a suspended phononic crystal with specially oriented line defects (aka waveguides) in it that split an incoming acoustic wave in two separate arms. The beam splitter is meant to operate in room temperature. The structure is designed to be made out of a high-stress Si3N4 membrane. The Phononic Crystal is created by etching circular holes in the membrane in a hexagonal pattern. A platform is created on which acoustic waves can be excited with a pulsed laser.

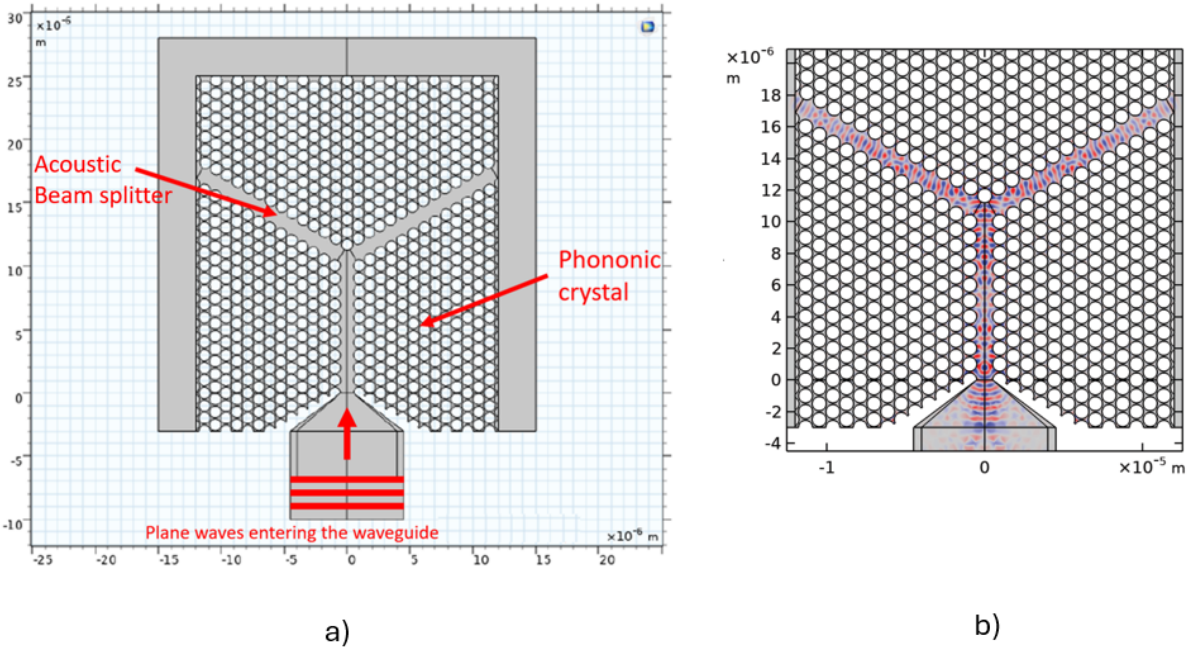

Figure 3: Design of a suspended Si3N4 acoustic beam splitter by M. van der Vis[15]. The design uses a phononic crystal to shield a waveguide structure. The structure serves as a splitter of incoming acoustic waves. a) shows the design. b) shows COMSOL simulation results of an acoustic wave being guided by the device

The beam splitter is designed to function around 3.5 GHz. Simulation results are presented in the Thesis, that study the "Energy confinement" of the Beam Splitter versus the PnC lattice; i.e. how much of the incoming wave energy stays within the line defect structure (aka Beam Splitter) versus how much of the energy dissipates into the Phononic Crystal lattice. Simulation results show about 85% energy confinement within the Beam Splitter for the hexagonal structure shown in Figure 3, indicating that the beam splitter design could be an efficient structure to transport an manipulate (split) GHz acoustic waves.

These simulation results gave the motivation for my thesis project to experimentally realize such a device, and the splitting of GHz acoustic beams on a suspended SiN waveguide. Such an experiment involves a very sophisticated laser setup to be able to excite and detect small acoustic waves in the waveguide. Therefore, parallel to designing and realizing such an acoustic beam splitter, a large portion of my work is dedicated to the measurement setup itself, and its capabilities to excite tunable acoustic waves on the waveguide and to be able to detect them even on longer travel distances.

2.3 Types of acoustic waves

Throughout this report, several references are made to the different types of acoustic waves. Therefore, a short overview is given here on the characteristics of these waves.

2.3.1 Lamb Waves

Lamb waves are a type of elastic wave that propagate in solid plates, exhibiting complex modes due to their dispersion characteristics. There are two main mode types: symmetric (S-modes) and antisymmetric (A-modes), as shown in Figure 4. Symmetric modes involve particle displacement that is symmetric about the mid-plane of the membrane, resulting in an even distribution of strain across the thickness. Conversely, antisymmetric modes exhibit particle displacement that is asymmetrical about the mid-plane, causing a bending or flexural motion in the membrane.

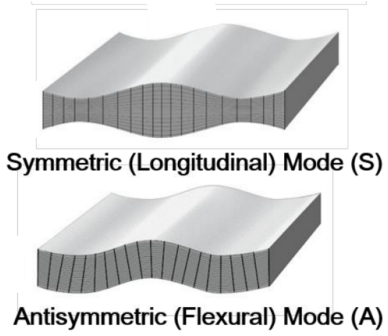

Figure 4: Symmetric (S-mode) and antisymmetric (A-mode) Lamb waves. Figure is presented by Sun et al. [21].

2.3.2 Rayleigh waves (SAW) and Love waves

A Rayleigh wave, also referred to as Surface Acoustic Wave(SAW) propagates along the surface of a material, as shown in Figure 5. Particles in this mode experience motion normal to the surface, making these types of waves more easily detectable than Love-mode shear waves, that only experience horizontal particle motion parallel to the surface.

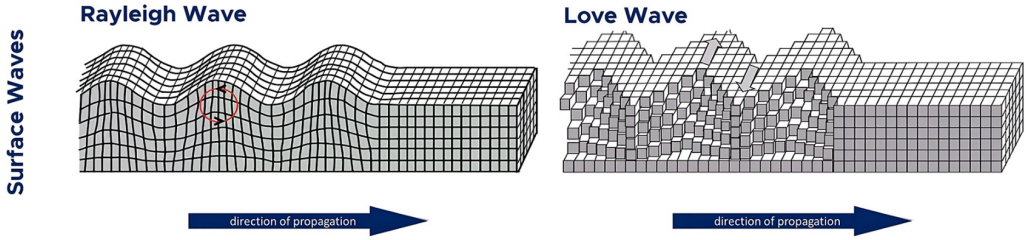

Figure 5: Rayleigh and Love waves Wikipedia [22]

2.3.3 Bulk Acoustic Waves

Bulk Acoustic Waves (BAW) are sound waves that propagate through the bulk or volume of a material. These waves eventually can reach the surface of a bulk material, thereby locally straining the surface out of plain.

This allows for detection of such waves by surface probing techniques. In BAWs, the two primary modes of propagation are longitudinal and transverse (shear). In longitudinal waves, particles in the medium move back and forth in the same direction as the wave is moving, creating compressions and rarefactions. In transverse waves, particles move perpendicular to the direction of wave propagation.

2.4 State of the Art: Laser excitation and detection of acoustic waves

In this section literature is reviewed that use laser setups to generate and detect tunable high frequency (surface) acoustic waves. Such laser pump-probe setups are often preferred because they allow for fast and non-intrusive testing of different samples and for the tunability of the excited acoustic waves on the sample. Special attention is payed to research that allows tunability of the excited SAWs, that is needed for the agile development of PnC based acoustic waveguides.

2.4.1 SAW creation with the help of periodically printed metal bars

In many state of the art ultrasonic photoacoustic experiments periodic metal bars are printed on the sample surface and heated with a pulsed laser. This periodic heating results in SAWs with a wavelength equal to the distance between the metal bars. Studies are summarized in this section that research this excitation method.

Surface acoustic waves in the GHz range generated by periodically patterned metallic stripes illuminated by an ultrashort laser pulse[23]

Bonello et al. used metal bars (Au and Al) heated by an fs laser pulse to create a periodic strain pattern on a substrate surface as shown in Figure 6. The strain pattern is created by the geometry of the metal bars that experience thermal expansion when excited with the pulsed laser (black arrow Figure 6).

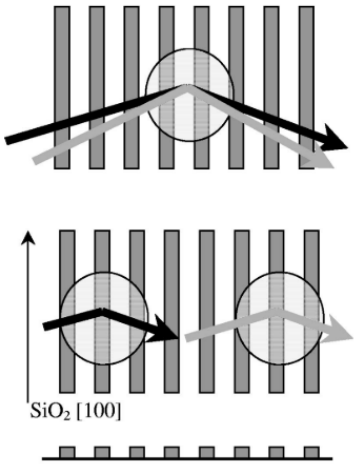

Figure 6: Geometry of the experiment. The dark rectangles represent the metal bars that were either gold or aluminium. The substrate was either silicon or quartz, see text. Black and grey arrows and circles around them represent the excitation laser spot and probe laser spot, respectively. The middle plot corresponds to the configuration in experiments proving that the SAW propagates outside the illuminated area.

The 100 fs laser pump pulse was used to excite the metal bars on the sample. A delayed probe pulse was used to measure the reflectivity of the surface. In most experiments, both pump and probe beams were focused at nearly normal incidence on the same area of the surface sample, with the diameter of the laser spot varying between 70 µm and 15 µm depending on the lens used.

The response from gold samples showed a single damped oscillation, the frequency of which did not conform to the expected Rayleigh wave at the surface of silicon. The frequency of this oscillation was found to be almost linearly dependent on the width of the metallic bars. The researchers suggest that this could be caused by the tight spacing between the gold bars ($1\mu m$) combined with the metal's high density.

The response from aluminum samples was notably different. Typical reflectivity responses with aluminum on silicon are shown in Figure 7 for different bar width. In these results peaks corresponding to the widths of the

metal bars are still present. Whats notable however are the frequency peaks corresponding to the period of the bar patterns ($1\mu m$). According to the researchers, the sharp peaks at 4.9 GHz are in good agreement to the expected SAWs with a $1\mu m$ wavelength in silicon. With this study the researchers proved that SAWs with pre-designed frequencies can be generated with the above described method.

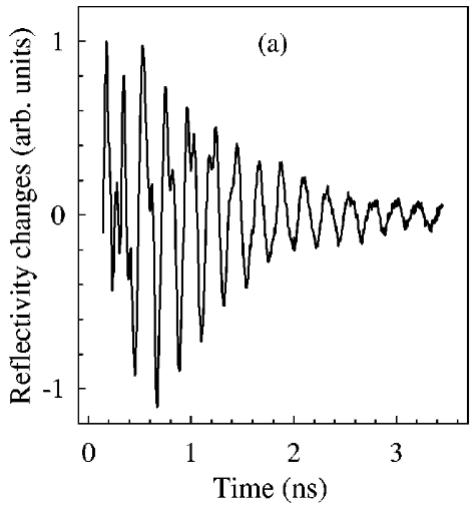

(a) Change in optical reflectivity as a function of time for a sample consisting of aluminum stripes 300 nm wide. A background of thermal origin has been subtracted. (b)

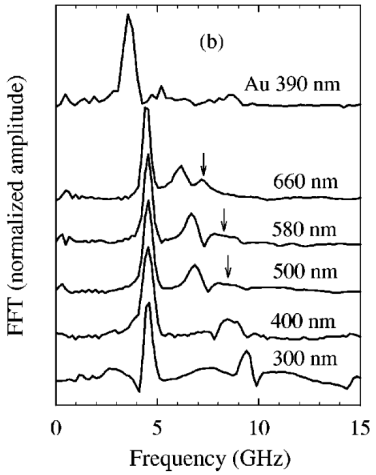

(b) Magnitude of the Fourier transform of reflectivity changes, for samples consisting of aluminum stripes on silicon. The spatial period is 1 um for all the samples. The arrows indicate the position of a likely normal mode. The Fourier transform of a gold sample (width of the metallic stripes: 390 nm) is plotted for comparison.

Figure 7: Results for aluminium stripes on silicon

Picosecond ultrasonic study of surface acoustic waves on periodically patterned layered nanostructures[24]

Colletta et al. report on generating and detecting surface acoustic waves (SAWs) using picosecond laser ultrasonics with a laser pump-probe setup. The pump pulse (an ultrafast ps laser) excites the sample comprising nanoscale Al lines on a SiO2 layer on a Si substrate. See Figure 8a. This leads to the rapid thermal expansion of Al lines and the generation of SAWs as seen earlier, which propagate perpendicular to the Al lines. The frequencies of these excited SAW waves range from 5 to 24 GHz, and in some cases, approach 50 GHz.

A probe pulse is used to detect these SAWs by the transient changes in reflectivity. The probe beam is focused on the same spot as the pump beam: the area where the Al lines are located. The pump laser has a 800 nm wavelength, while the probe has either 400 or 800 nm wavelength. SAW's were recognized by their expected frequencies that depend on the pitch p of the Al lines. It was observed that sensitivity is strongly dependent on the polarization of the probe beam: S-polarized probe is more sensitive to GHz frequencies. This polarization dependent sensing could be attributed to the electric field complexities around the Al lines on the substrate.

Ten different samples were analyzed, varying in pitch (1000 to 140 nm) and SiO2 film thickness (either 112 nm or 60 nm).

Figure 8b shows the Fourier transform of recorder reflectivity change signals for samples with d=112 nm and p= 400nm and 200nm. It is clear from the results that for a smaller fringe spacing p, a higher SAW frequency response is excited. Temporal responses showed that for the 200 nm pitch sample the vibrations were shorter lived: this is probably due to the added mass that is added to the surface due to the tighter spacing of the metal bars. This directs more acoustic energy into the bulk of the sample.

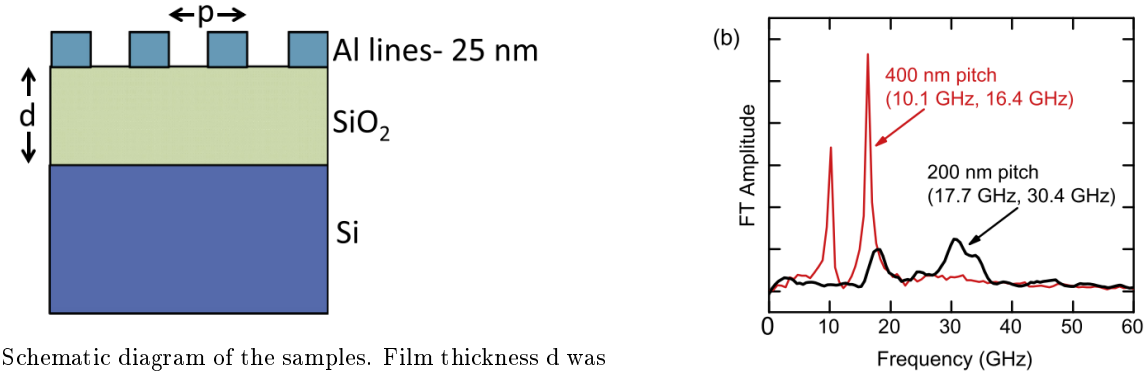

(a) Schematic diagram of the samples. Film thickness d was either 60 nm or 112 nm as measured by picosecond ultrasonics. Al lines pitch p varied from 1000 nm down to 140 nm. The duty cycle was close to 50% (±10%) in all cases as measured by SEM imaging

(b) Fourier transform of measured surface reflectivity change(ΔR)signals for two samples with d=112nm and p=400nm and 200nm

Figure 8: Sample and results of measurement

2.4.2 Tunable SAW excitation with the creation of light interference patterns on the sample surface

In this section methods are presented from state of the art studies that apply different techniques to create pump laser interference patterns on the sample. Shaping the interference pattern results in tunable SAWs.

Laser-induced transient grating setup with continuously tunable period[26]

A. Vega-Flick et al. used laser-induced transient grating spectroscopy to generate surface acoustic waves in a sample. They report on achieving continuous tunability of the grating period on the sample surface. This allows for fine-tuning the frequency of the surface acoustic waves that are excited in the sample. The setup is shown in Figure 9a. The pump and probe beams are split into diffraction orders by a phase mask (diffraction grating) and focused on the sample surface, thereby creating an interference pattern. Tunability is achieved by rotating the diffraction grating as shown in 9b. By rotating the mirror, the angle of diffraction orders can be manipulated. The setups use sub-nanosecond 532 nm laser pulses and a continuous-wave probe beam. The probe beam is optically heterodyned in the sample and detected with a photodiode behind the sample. The sample in the study is a 100 nm Aluminium film deposited on float glass substrate.

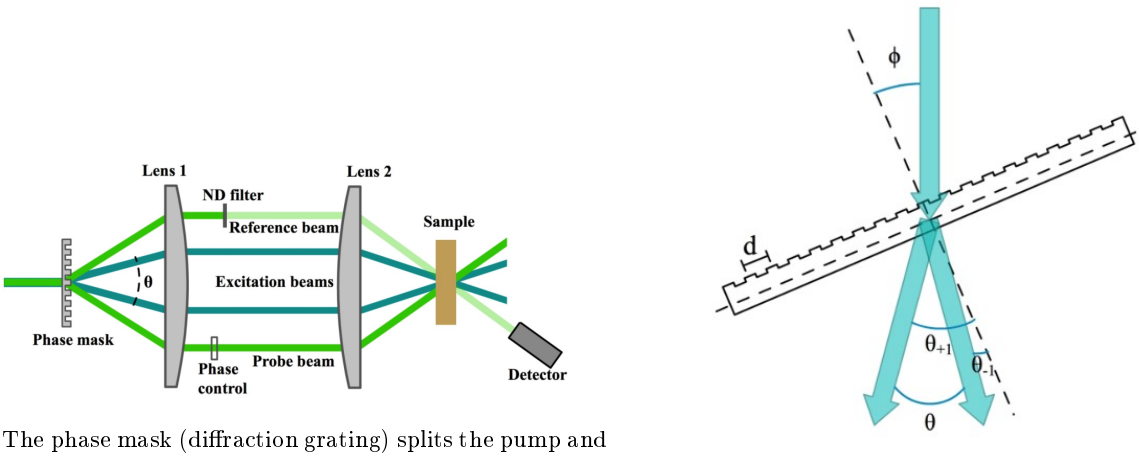

(a) The phase mask (diffraction grating) splits the pump and probe beams under a certain angle. The angle of incidence of the pump beams on the sample surface determines the fringe pattern, i.e. excitation frequency.

(b) Tunability of the excitation frequency is achieved by rotating the diffraction grating, thereby changing the angle of incidence of light on the sample surface.

Figure 9: Experimental setup used by A. Vega-Flick et al. [26]

Experiments conclude that the tilting of the phase mask indeed decreased the TG(fringe) period: a tilt from

0° to 25° decreased the TG period from 11.5 μm to 10.42 μm. This translates into an tunable SAW excitation frequency between $270 - 305 MHz$. These results are shown in Figure 10. For

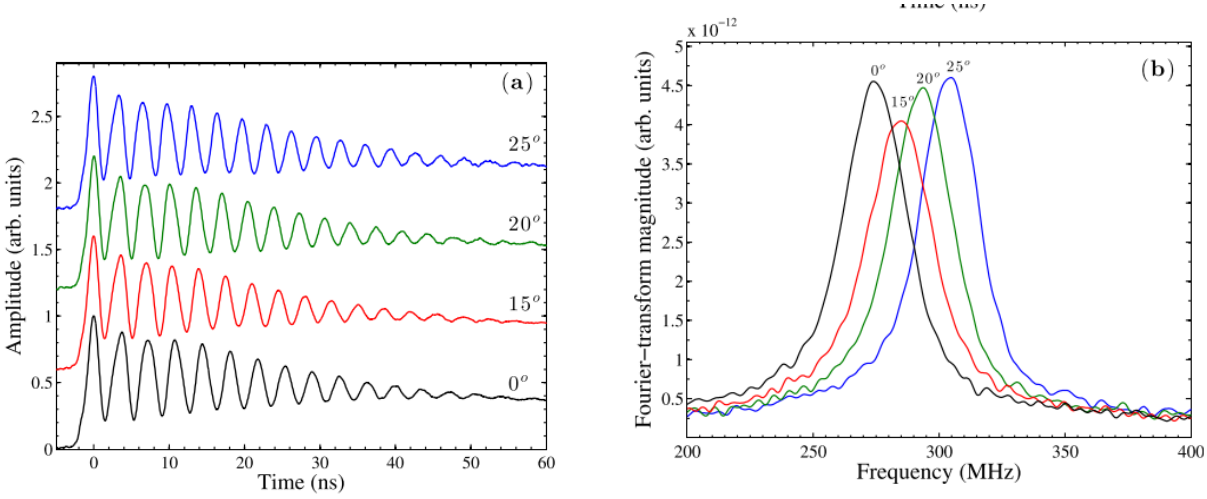

Figure 10: (a) Measured signals obtained for the Al-coated glass sample, at transient grating period of 11.5 µm (for 0°*tilt*) and tilt angles from 0° to 25°. (b) Fourier spectra of time traces in (a)

Researches presented a setup that successfully and easily can manipulate the frequency for SAWs it excites by just the the tilting of a diffraction grating with 532 nm sub-nanosecond excitation lasers.

Generation and detection of tunable phonon polaritons using a single transmission grating[27]

Katayama et al. used the transient grating method to excite phonons in a $LiNbO_3$ sample in a spatial periodic pattern. The goal was to be able to tune the periodic spacing of light and dark fringes on the sample. The setup is shown in Figure 11a. Coherent light is shown onto a transmission grating after being passed through a lens. The sample ($LiNbO_3$) is placed a distance d behind the focal position. This way a fringe pattern appears on the sample surface. By varying distance D, this image can be expanded or reduced, thereby changing the distance between the light and bright fringes on the sample. A 150 fs laser was used at a wavelength of 775 nm. Figure 11b shows images of the fringes created during the experiment. As can be seen, the spacing between the fringes is varied for different grating positions (distance D). The researchers managed to vary the fringe spacing between $52 - 460 \mu m$.

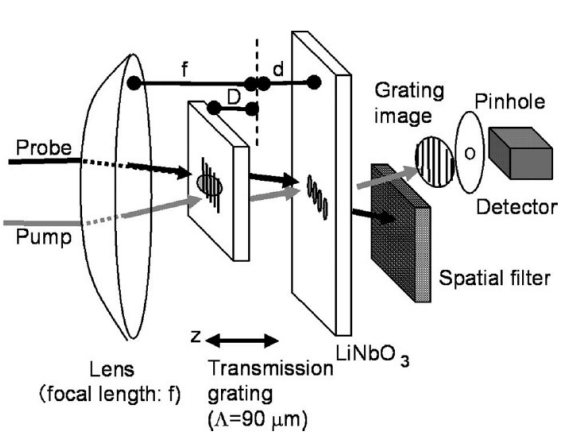

(a) Optical setup of the experiment.

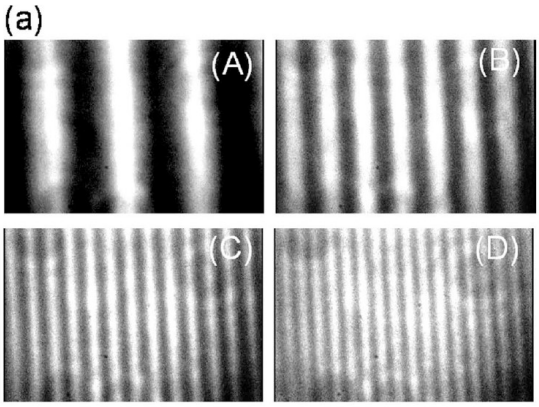

(b) Grating images (A to D) for different sample-grating distances

Figure 11: Optical setup and the resulting fringe patterns on the sample, created with an original application of the transient grating method, presented by Katayama et al. [27].

2.4.3 SAW excitation with a Gaussian pulsed laser spot

This section present a study that shows how a simple Gaussian pulsed laser spot diameter is related to an excited SAW frequency, thereby allowing the tunable creation of SAW by manipulating the laser spot size.

Time- and frequency-domain characteristics of laser-generated ultrasonic surface waves[28]

Scala and Doyle establish a quantitative basis for the application of laser-generated ultrasound in the thermoelastic regime. The focus was on the generation of longitudinal shear and Rayleigh waves by laser pulses on solid surfaces. A Q-switched Nd:YAG laser system was used for generating elastic waves, that were then detected by a wideband piezoelectric sensor, as shown in Figure 12a The excitation laser pulses had a duration of about 25 ns and an energy ranging from 5 to 80 mJ. The laser beam had a Gaussian profile with a half-width parameter 'a'. A theoretical model was also made to be able to compare with experimental results. A typical measured wavefront in the farfield (r=50 mm) is shown in Figure 12b.

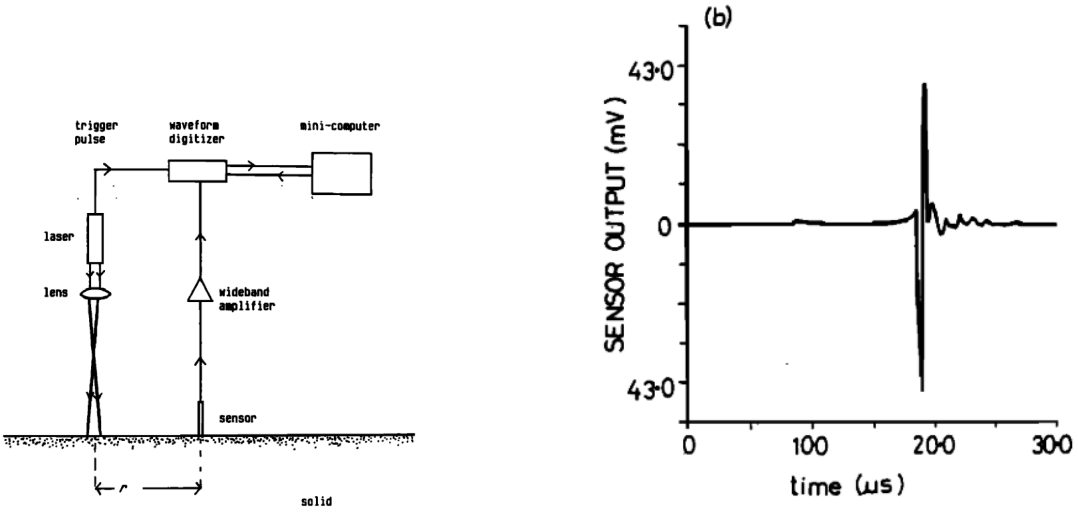

Figure 12: Experimental setup and results of surface acoustic wave generation by Scala and Doyle[28]. a) Experimental arrangement for surface acoustic wave generation using. The source and sensor are a distance r apart. b)Surface waveform at the far-field for spot size a=0.5 mm and sensor distance r=50mm. The sensor output shows the displacement of the piezoelectric sensor.

The study demonstrated that the highest Rayleigh wave peak frequency and bandwidth occurred when the Gaussian laser beam's half-width 'a' was reduced just enough to begin surface damage. It was also found that for a decreasing excitation spot size 'a' both the bandwidth and peak frequency increases. This is shown in Figure 13. The peak frequency was determined by evaluating the time separation of the dipolar Rayleigh wave peaks shown in Figure 12b. It was also observed that in the near-field, the bulk pressure wave (sP) overlapped the Rayleigh wave and contributed more significantly to the observed waveform than in the far-field.

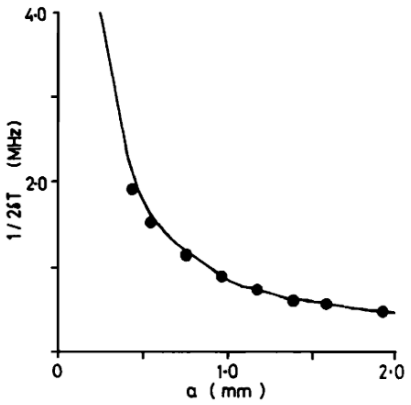

Figure 13: Variation with laser beam half-width a of $1/(2\delta T)$, where δT is the time separation between the dipolar peaks of Rayleigh waves in the farfield thermoelastic regime for $r = 50$ mm. The solid line represents the theory. The experimental results (black dots) are for a laser energy of 30 mJ, except for the lowest a used (at 0.45 mm) where a reduced energy of 12 mJ was chosen to maintain a predominantly thermoelastic source.

This study generated SAWs in the low MHz range that is much lower than what our suspended wave splitters will carry. However, the experiments proved that if the laser spot size is varied, the generated frequency can be manipulated.

2.4.4 Beam Distortion Detection

In the presented studies above, some applied reflectometry to detect acoustic waves on the sample surface. This is done by shining a probe laser on the sample surface and measure the changes in the reflected light intensity. In this section a similar, but for some applications more sensitive, method is presented called Beam Distortion Detection (BDD). This method is very similar to a reflectometry laser setup: the difference is the presence of a diaphragm in front of the detector.

Surface displacement measured by beam distortion detection technique: Application to picosecond ultrasonics[29]

Chigarev, Rossignol, and Audoin present a surface displacement measurement technique called Beam Distortion Detection (BDD), used for picosecond ultrasonics. This method offers a sensitive non-contact approach for detecting short acoustic pulses, created by low-energy laser pulses.

The schematic of the BDD setup is shown in Figure 14. When the sample is excited with a pump laser, the sample surface deforms due to thermal expansion, causing a surface curvature to appear. Because the probe laser is directed to this same surface, the surface curvature changes the angle of divergence of the reflected probe beam, thereby changing its radius a at the diaphragm. This way, the power that goes through the diaphragm changes. This change is detected by a photodetector.

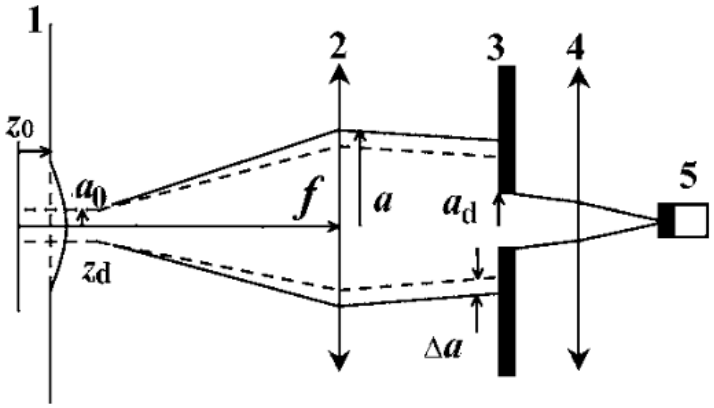

Figure 14: The schematic of BDD techniques. 1—sample, 2—objective, 3—iris diaphragm, 4—focusing lens, 5—photodetector.
$a_0 \approx 0.5\mu m$ radius of the deromation area, $a \approx 0.5\mu m$: radius of the probe beam on the objective, $\Delta a \approx 100pm$: the change of the probe beam radius, $a_d \approx 0.5mm$: radius of the diaphragm, $f \approx 2mm$:—focal length of the ob- jective, z_0:position of the sample surface, and $z_d \approx 1\mu m$:the diffraction length

The BDD method was experimentally tested on a silicon substrate coated with a 450nm gold layer. Results were compared to interferometric and reflectometric detection methods, as shown in Figure 15. The BDD method detects the acoustic echoes just as well as the interferometric setup, but with 10 times faster acquisition time to reach the same signal-to-noise ratio. Reflectometric detection without the diaphragm proved to be much less sensitive as it did not capture the acoustic echoes.

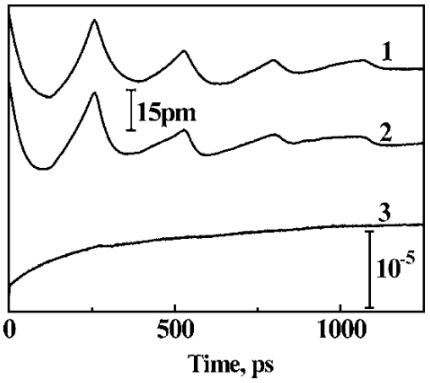

Figure 15: Optoacoustic signal in the gold layer at $\approx 0.45\mu m$ thickness on silicon substrate. 1) interferometric signal, 2) reflectivity signal with the diaphragm, and 3) reflectivity signal without the diaphragm.

Efficiency of this method is especially good when the sound wavelength is long relative to the area of light absorption. Because this method is applicable to setups with a normal angle of incidence, it is simple and efficient for detection of surface displacements.

2.5 Conclusions of State of the Art research

2.5.1 Excitation methods

Literature has shown that fast pulse laser pump-probe setups are capable of generating GHz SAWs, while also influencing the excited acoustic frequency spectrum (tunability).

A simple way to achieve tunable SAWs is done in a study that shows how the diameter of a simple Gaussian laser spot effects the excited SAW frequency. [28].

In more recent studies that use femtosecond to nanosecond pulse lasers to generate tunable SAWs in the GHz range, two main methods are used:

1. Manufacturing thin periodic metal bars on the sample surface and heating them with a single laser spot. [23][24]
2. Creating a laser interference pattern on the sample surface. [26][27]

In both cases the result is a spatially periodic strain pattern on the sample surface caused by the photoacoustic effect. This strain pattern spreads in the form of SAWS along the surface of the substrate, with a wavelength determined by the distance between the strain patterns, and a direction defined by the orientation of the fringes.

Printing metal bars is not preferred in this project, as it complicates manufacturing and requires many different design variations to be able to generate SAWs at varying frequencies.

Using interference patterns and being able to manipulate the distance between the interference fringes carries the advantage of non-intrusive tunable SAW excitation.

Katayama et al. [27] presents a femtosecond laser setup with the above mentioned capability, by placing a transmission grating between the focusing lens and the sample. However, this setup is not a reflectometry setup and it only functions with a transparent sample, thereby excluding SiN membranes. Vega-Flick et al. [26] also present a tunable SAW setup using a diffraction grating to create the interference patterns. However, here relatively slow nanosecond lasers are used. For a femtosecond laser setup, such a diffraction grating solution requires very precise alignment of the optical components ($+-30\mu m$).

The above considerations define a knowledge gap in how to create tunable SAWs with a femtosecond reflectometry pump-probe setup, as such a setup has not yet been presented in literature.

2.5.2 Detection methods

The most commonly used detection method in literature, that can be used in combination of opaque samples like SiN membranes, is reflectometry. A probe laser is shown on the sample surface, and the reflected probe beam is picked up by a detector. Acoustic waves can then be detected by looking at transient changes in the measured reflectivity of the sample. Another similar, but in some applications more sensitive method is presented by Chigarev et al. [29] that use Beam Distortion Detection (BDD) to detect acoustic waves. This method can easily be applied to reflectivity measurement setups by adding a diaphragm to the reflected probe beam. It shows improved sensitivity to acoustic waves that curve the sample surface out of plane. Important to note, that a BDD signal purely relies on geometrical features of the sample surface, while a reflectivity signal is mainly influenced by the photoelastic coefficient of the sample. When the BDD method is applied by adding a diaphragm to the setup, the resulting measurement signal is essentially a combination of these two methods.

3 Method

In the Method section the relevant topics of the Thesis Project are prepared and presented. These include:

1. The measurement setup. Capabilities of the available femtosecond laser pump-probe setup needed to be investigated and developed, to be able to determine if and how it can successfully test a manufactured Si3N4 suspended acoustic beam splitter. This includes the approaches to create tunable SAWs on a sample surface and be able to measure them at larger distances.
2. Design of the phononic crystals and acoustic waveguides, and splitters with the help of COMSOL simulations.
3. The final designs of acoustic waveguides, splitters and other structures.

3.1 Measurement Setup

Excitation and measurement of the acoustic waves on the sample is done with a femtosecond pulse laser pump-probe setup based on the reflectivity/BDD method discussed in Section 2.4.4. The schematic of the setup is shown in Figure 16. The core setup used in this study is developed by M. Robin and R. Guis et al [16] at TU Delft. However, there are some differences in the current setup compared to the one described in the study. The differences in the setup are:

1. The absence of a birefringent crystal
2. The presence of a balanced photodetector, combined with a reference arm of the probe beam. These are used to greatly increase sensitivity of the setup by subtracting the background level/optical noise (reference arm) from the probe beam.
3. For some experiments, a mask is placed in the pump beam path to create interference patterns on the sample. This method is described later in this section.

The pump laser is focused on the sample surface, where an absorbing top layer absorbs a part of the laser energy, thereby creating acoustic waves in the membrane due to the thermal stresses caused by the laser. The probe laser is focused on-, and reflected back from the sample surface and guided to the photodetectors. A Diaphragm is placed in the probe beam path just before the photodetector to apply the BDD method[29]. The other photodetector picks up the reference signal, so that the balanced photodetector can differentiate the probe and reference signals and output the difference. The changes in this light intensity directly correlates with the amplitude of the acoustic waves on the measured surface. The pump and probe lasers are locked together with a small repetition rate difference Δf. Because of this small frequency offset (kHz vs MHz), the probe pulse slowly scans through the signal , allowing the capture of a high resolution 10ns signal within $\frac{1}{\Delta f}$ time. This method is called Asynchronous Optical Sampling (ASOPS) and it is used to reach a high temporal resolution of the signal.

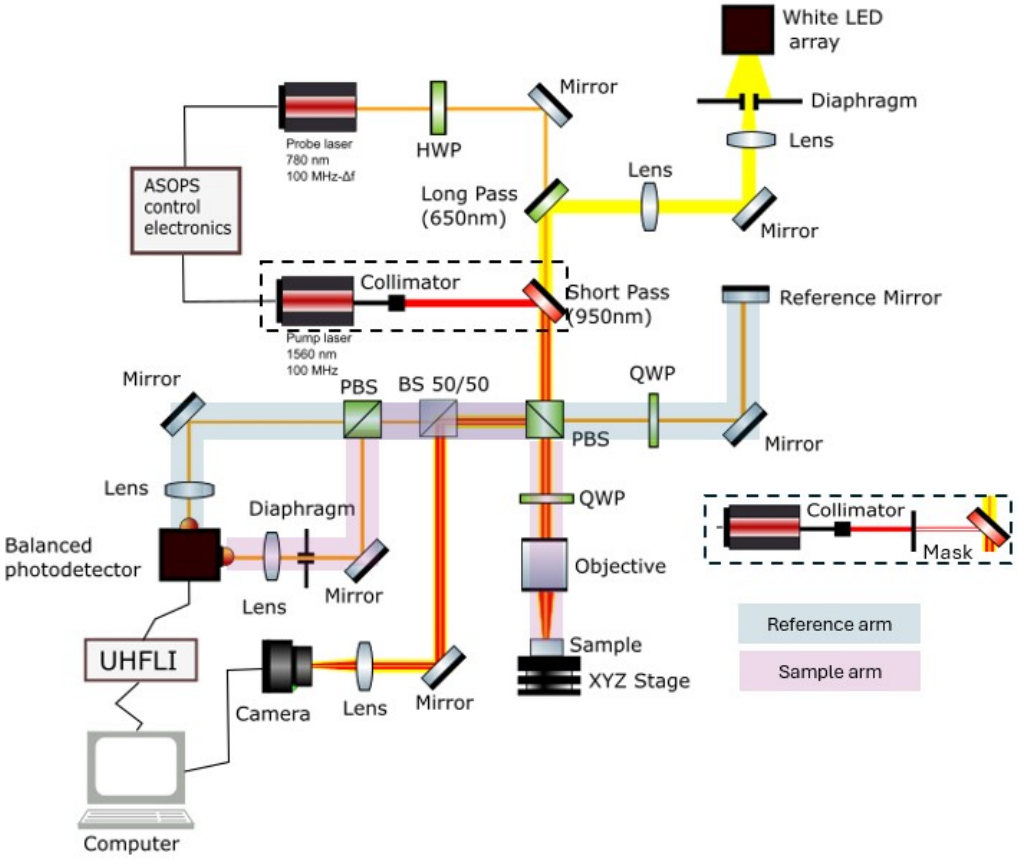

Figure 16: Ultrasonic pump-probe ASOPS setup with BDD detection built by M. Robin and R. Guis [16] HWP: Half-Wave Plate, QWP: Quarter- Wave Plate, (P)BS: (Polarizing) Beam Splitter, Long Pass/Short Pass dichroic mirrors (cut-off wavelength). A Balanced Photodetector is used to output a differential signal of the reference arm (blue shaded) and the sample arm (pink shaded) of the probe laser. A diaphragm is placed in the sample arm to apply the BDD principle. A camera and white LED array is used to align the probe and pump lasers on the sample surface.

3.1.1 Pump laser path

The Erbium Menlo Systems pump laser is used to periodically heat up the sample surface, causing acoustic waves in the membrane due to the thermal stresses. The 1560nm laser has a pulse duration of about 100 fs, a repetition rate of 100MHz and an average output power of about 100 mW. After leaving the collimator, the free-space pump laser beam is directed towards the sample surface with a Short Pass dichroic mirror. After a PBS and QWP, the beam is focused on the Sample by a Mitutoyo Plan-Apochromat objective (M=20). The pump spot has a diameter on the sample surface of about 7-8 um.

3.1.2 Mask

In Section 2.4 it has been discussed that creating an interference pattern of the excitation laser on the sample surface allows for the tuning of the excited acoustic frequencies. There are several methods to concentrate the light energy into spatially organized lines (fringes). A common method to achieve this tunable wave excitation is to use diffraction gratings to split the pump probe in diffraction orders and focus the separate orders on the sample surface. However, because of the large wavelength of the pump laser (1560nm) in this setup, using a diffraction grating poses great technical challenges because of the resulting large diffraction angles. Furthermore, the short (100fs) pulses would require extremely precise ($+-30/mum$) alignment between the diffraction order beam paths, posing even more technical challenges.

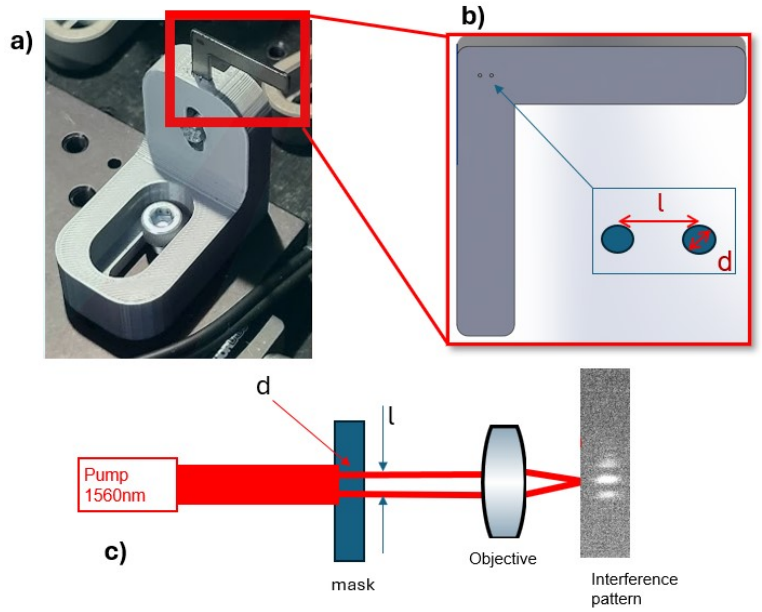

Figure 17: a) 3D printed mask holder and L-shaped mask. The masks are L shaped so that the orientation of the can be rotated 90 degrees. b) CAD model of a mask and its parameters c) Working principle of the mask: the mask trims the incident laser beam profile into the shape of the holes on the mask. The resulting two beams creative positive and negative interference lines on the sample surface. Parameters d and l make it possible to tune the size and fringe distance of the resulting pattern.

Therefore it was decided to use masks that trim the beam profile to the desired shape. Applying a mask in the pump beam path can be easily done without changing the rest of the setup, making it an attractive choice. The mask is a simple laser cut steel sheet, with two hole in it. See Figure 17. The holes are placed in the laser path, thereby trimming the beam to the shape of the holes. In the case presented in Figure 17, the holes consist of two circles. This way two coherent, collimated laser beams are created. When these two beams are focused on the sample by the objective, an interference pattern appears. This interference pattern depends on the hole diameter d and distance hole distance l, and can be calculated by taking the spatial Fourier Transform of the real space beam profiles created by the mask.

3.1.3 Probe laser path

Similarly to the pump laser, the probe laser is also an Erbium laser made by Menlo Systems, with a 100fs pulse duration, but with a smaller wavelength of 780 nm. The average emitted laser power is around 5-7 mW at the laser output and around 1 mW at the photodetector. The beam path goes through a Half-Wave Plate to maximize efficiency of the PBS, that splits the probe beam into a sample arm and a reference arm. The sample arm is then focused on the sample surface (and reflected back from it), while the reference arm is reflected from a simple reference mirror. After reflection, both the reference arm and the sample arm are passed through twice a QWP to rotate their polarisation and to then be directed by a PBS into the Camera and the Photodecetor. A second PBS seperates the sample and reference arms before they are both detected by the Balanced Photodetector. The sample arm, before it reaches the Photodetector, is guided through a Diaphragm that enforces the BDD method by trimming edges of the beam.

3.1.4 Data acquisition

Similarly to the method described by M. Robin and R. Guis et al [16], the signal of the Balanced Photodetector is processed by an Ultra High Frequency Lock-In (UHFLI) amplifier (Zürich Instruments, 600 MHz bandwidth). Herein, the Boxcar and PWA functions of the amplifier are used to reconstruct the probed acoustic signal. The Boxcar (i.e. Gate) function is used to determine which sampled readings of the detector are part of the signal. The PWA function is used to put these samples in the correct order and reconstruct the signal.

3.2 Integration experiments

The goal of the project is to experimentally design a GHz acoustic beam splitter and a compatible measurement setup. Before designing the beam splitter, several questions needed to be answered that required experiments. Some of these questions relate to the design itself, some relate to the laser pump-probe setup described in Section 3.1. The most important questions were:

1. Setup capabilities for SAW excitation and measurement: in what frequency range is the setup capable of exciting and measuring GHz SAW's and over what wave travel distances?
2. Tunability: Is it possible to tune the excited SAW frequencies to match them with the bandgap of the PnC?
3. Material: how do different materials used as a coating enhance measurement sensitivity?

For all of these tests simple suspended membranes were used, that do not include waveguides. See Figure 18. All of these membranes have a periodic hole pattern structure with a square lattice pattern. The holes are needed for manufacturing purposes: to etch away the SiN substrate under the membrane and thereby suspending the structure. The lattice constant of these 2D PnCs is equal to 3.5um and the hole diameter is 1.5um. Membranes were used made out of SiC and SiN. The SiN membranes are coated either with Au or NbTiN.

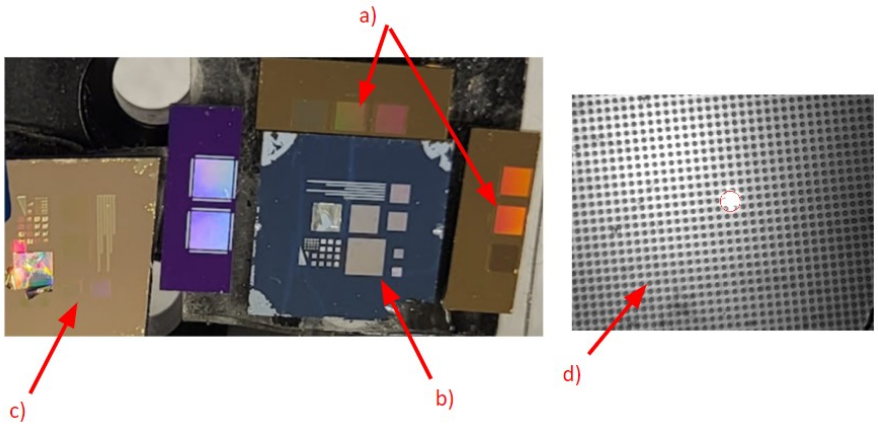

Figure 18: Suspended membranes used for the tests described in this section. The membranes are made of different materials and coatings. a) 45nm NbTiN coating on 340nm SiN membrane. b) SiC membrane c) 45-70nm Au coating on 340nm SiN membrane d) image of sample: all of these suspended membranes have a square lattice pattern of circular holes. The lattice constant of the membrane is 3.5 um and the hole diameter is 1.5 um.

3.2.1 Setup capabilities for SAW excitation and measurement

The laser pump-probe setup described in Section 3.1 used for this research was originally built to excite and measure Bulk Acoustic Waves. Therefore it had to be investigated if the setup is capable of exciting and measuring Surface Acoustic Waves, even on longer acoustic wave travel distances. For these experiments the gold membranes were used shown in Figure 18. The strategy for the test is depicted in Figure

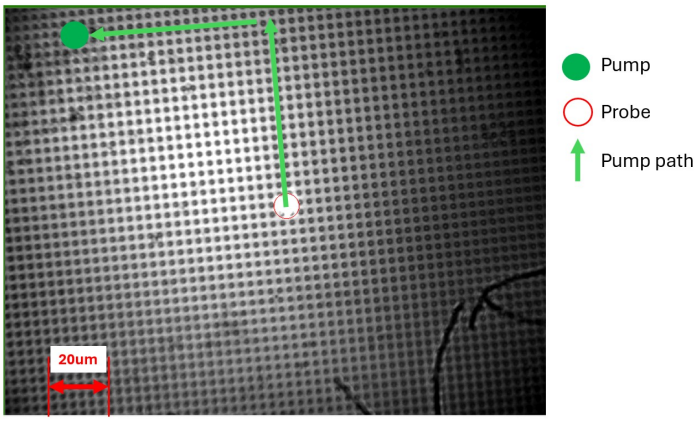

Figure 19: Image of the Au coated SiN membrane. Red circle indicates the location of the probe laser spot. The green circle indicates the pump laser spot. The green arrows indicate the path of the pump spot for the different measurements. For the first measurement the pump spot coincided with the probe spot. Then step by step it was moved away from the probe spot along the green lines.

By changing the distance between the pump and probe spot the goal is essentially to find the limit where the setup still can detect a signal. Also, studying the amplitude and frequency changes in the measured SAWs at different locations could tell us valuable information on the behaviour of these acoustic waves.

3.2.2 Tunability experiments: interference pattern and spot size manipulation

Simulations help approximate the bandgap of a PnC. However, manufacturing imperfections and simulation limitations can result in a different PnC bandgap, than expected. Also, to characterize the manufactured PnC, it is important to be able to excite varying frequencies that fall inside bandgap and modes that fall outside the bandgap. It is therefore important to be able to "tune", i.e. manipulate the excited acoustic wave frequencies to experimentally be able to match the phononic bandgap of a PnC. In this research two methods were tested that potentially allow the manipulation of the excited frequencies:

1. Interference pattern creation on the sample surface
2. Spot size variation of the pump (and probe) laser spot

1. Interference pattern creation on the sample surface

In the presented Sate of the Art cases in section 2.4 it has been shown that a proven method of manipulating the excited acoustic frequencies is to create a periodic strain pattern on the sample surface, i.e. focus the laser energy in a repetitive pattern of lines on the sample surface. The distance between the lines then defines the wavelength (and frequency) of the excited acoustic waves. Some studies [26][27] achieved this in a way that allows manipulation of the distance between these lines, i.e. to tune the acoustic frequency. This can be done by creating an interference pattern on the sample surface by focusing two parallel, coherent laser beams on the sample surface. The spatial profile of the parallel beams (i.e. the shape of the apertures of the mask) determine the resulting interference pattern. The interference pattern can be calculated by taking the Spatial Fourier Transform of the spatial profile of the apertures.[30] [31].
A femtosecond laser poses a challenge for this method. Creation and alignment of two collimated beams is challenging. After splitting the laser beam in two separate arms, even very small laser path length differences would result in the two pulses arriving at the sample surface after each other, thereby not creating any interference pattern.

To avoid this alignment problem, masks are used that trim the pump beam to two separate beams, as shown in Figure 20a. The masks are made of sheet metal. Two apertures are cut in each of them with varying geometries. A 3D printed mask holder was made, see Figure 20b that allows for easy and precise change of masks without needing any further re-alignment. Several masks were laser cut from sheet metal with different aperture geometries to be able to test the working principle.

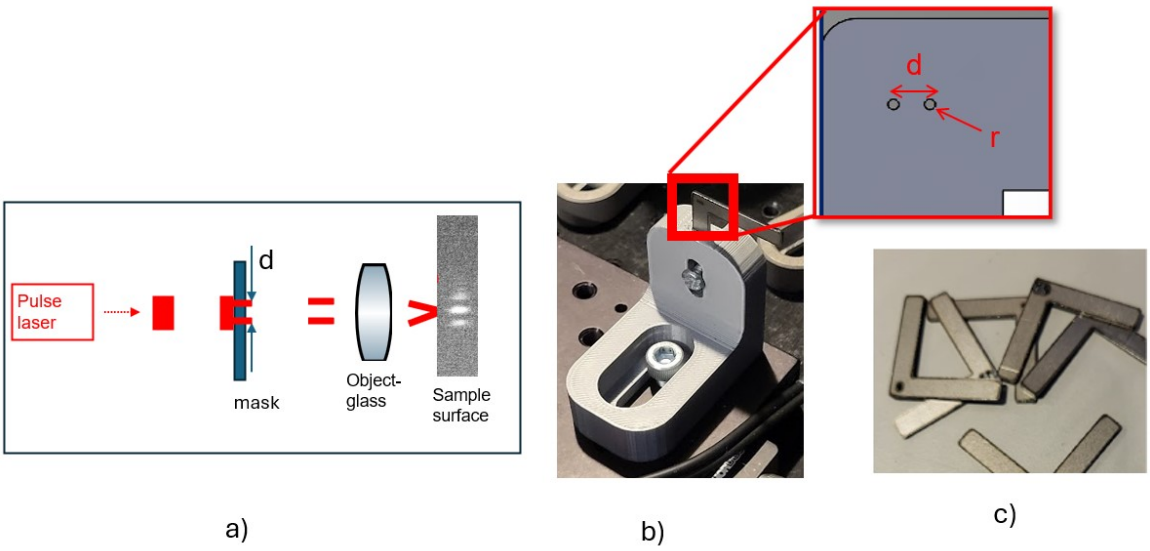

Figure 20: a) Schematic of the working principle of how masks create interference pattern on the sample with a pulsed laser. The repetitive red lines represent the traveling laser pulses. Distance d between the holes on the mask determine the fringe spacing on the sample. b) Mask holder installed in the optical setup, that allows for easy and fast swap between different masks. Zoom-in inset shows the apertures on the mask and its relevant parameters. c) A collection of masks with varying aperture geometries.

The masks were tested first with the probe laser beam because the camera is not so sensitive to the pump laser wavelength. Later the pump beam was also tested with the masks. The goal was to confirm that interference patterns can be created on the sample surface with these masks, and that the different masks result in changing interference patterns. It was also the goal to check if the masks change the acoustic frequency spectrum on the sample. See the results of these tests in Section 4.1.2

2. Spot size variation of the pump (and probe) laser spot

In literature it has been shown that the spot size of a laser spot can have an influence on the excited SAW frequency in the sample[28]. Since laser spot size can easily be manipulated by shifting the laser spot slightly out of focus, this method could potentially be a simple way to tune the excited frequencies. Tests were performed on the gold coated SiN membranes, shown in Figure 18, where the focus was adjusted step by step, and the resulting acoustic waves were analysed for their frequency components.

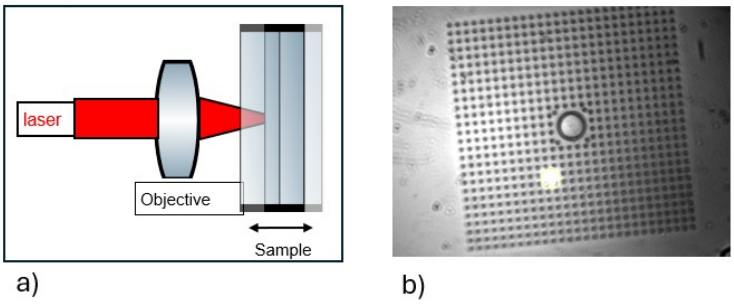

Figure 21: a) Schematic that shows how shifting the sample around the focus point of the objective changes the laser spot size on the sample surface b) Image of the sample membrane, showing the probe spot. The sample is a 100x100 um 2D Au coated SiN PnC with a=3.5 and d=1.5

3.2.3 Material experiments

Several materials were tested with the setup to see which material gives the best signal. In Figure 18 the different suspended membranes are shown (a-c), and the membrane lattice they are made of (d). The expectation is that a metal coating will be needed to absorb enough heat to generate large enough acoustic waves. For these tests, the pump and probe beams were aligned, meaning that the location of the excitation and probing spots were overlapping.

SiC membranes and 340nm thick SiN membranes with 45-70 nm thick NbTiN or Au coating were tested. The SiC membranes, as expected, did not result in any measurable signal, as SiC is very transparent to 1580nm light.

3.3 Phononic Crystal Design

In order to design the suspended acoustic waveguide and splitters, careful design of the phononic crystals surrounding the waveguides is needed. In this section the method is presented on how this shall be achieved. First, the COMSOL bandgap simulation is validated with results found in literature. Then, the crystal lattice used by M. van der Vis[15] is compared to a potentially better functioning crystal lattice (Shamrock-type lattice). Finally, the requirements for the final PnC designs are outlined.

3.3.1 Bandgap Simulation Validation

The simulation of the phononic bandgaps was conducted using COMSOL Multiphysics. How this is done, is in detail explained in the Thesis of M. van der Vis[15], but also on the website of COMSOL[32]. To assure that the built up simulation in COMSOL works well, a phononic crystal design based on the parameters used in the experiments of Florez et al.[12] was compared. In the paper, a bandgap ranging from 6,7 GHz to 11,4 GHz is presented.

The bandgap of the simulation is shown in Figure 22. A bandgap ranging from 6,4 GHz to 12,3 GHz is shown, which is in good agreement with the results of the above mentioned paper.

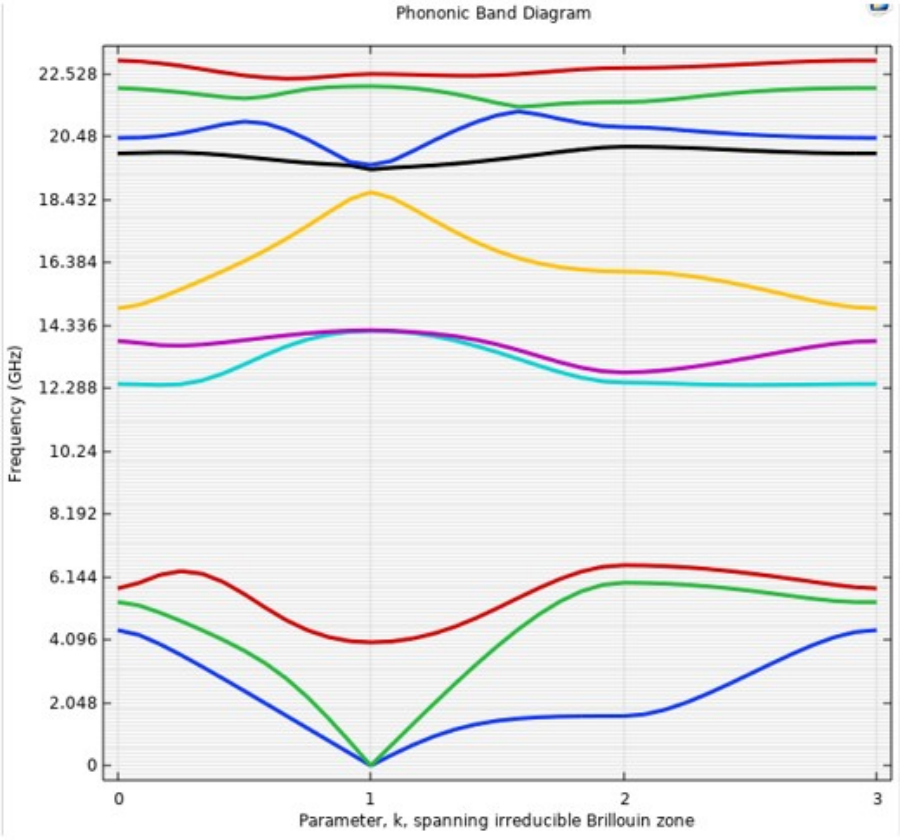

Figure 22: COMSOL Simulation results of a phononic crystal based on the parameters presented in the work of Florez et al.[12]. The simulated bandgap is in good agreement with the bandgap reported by Florez et al, thereby raising confidence in the simulation's ability to help design the phononic crystals for the waveguides.

3.3.2 Phononic Crystal Lattice Comparison

The primary objective was to design the bandgap as large as possible, due to the uncertainties around what the actual excitation frequencies will be. Hexagonal lattices are used, as such lattices could more efficiently be used to create acoustic wave splitters, than square lattices[15].

Shamrock patterned and simple hole patterned phononic crystals are compared based on bandgap simulations results, both crystals in a hexagonal orientation. The Shamrock pattern was chosen because of the promising results presented by Florez et al.[12]. The circular pattern was studied to optimize the waveguide designs presented by M. van der Vis[15]. See Figure 23 for the two compared lattice types and their relevant design parameters.

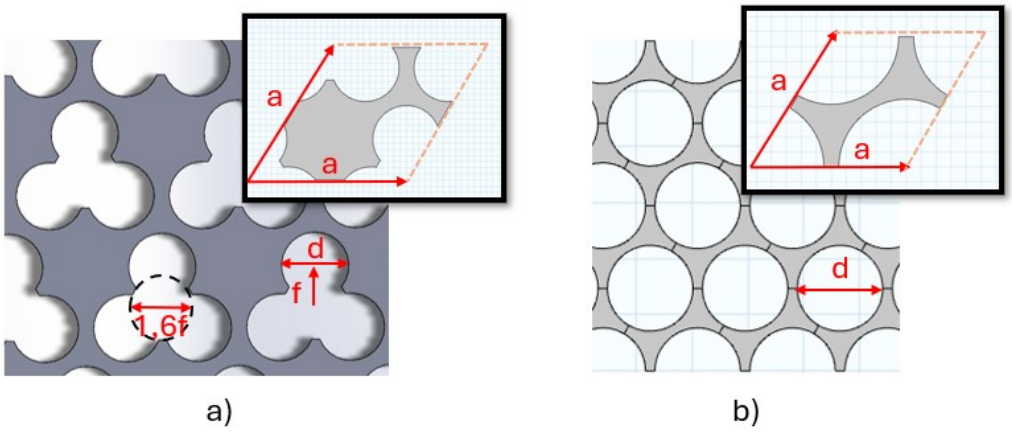

Figure 23: a) Shamrock-type PnC lattice, with design parameters a, f and d. Inset shows the basic unit cell of the hexagonal lattice. b) Circular PnC lattice with design parameters a (lattice constant) and d (hole diameter). The inset shows the basic unit cell of the crystal.

	Shamrock	**Circular**
a (μm)	10	10
d (μm)	$0.44 * a$	9
f (μm)	$1.05 * d/sqrt(3)$	

Table 1: PnC lattice parameter values for the bandgap comparison of the circular and shamrock type crystals.

The parameters of these crystals were tuned by trial and error in a way to approximately match their largest bandgap centers with each other. The found parameters are listed in Table 1. Simulations were made where the center of the largest bandgap in both cases is around 0.55 GHz. To compare the bandgaps the gap-to-midgap ratio used [12][15] that is defined by the following equations:

$$\Delta\omega = \omega_u - \omega_l \tag{1}$$

$$\omega_m = \frac{\omega_u + \omega_l}{2} \tag{2}$$

$$\text{Gap-to-Midgap Ratio} = \frac{\Delta\omega}{\omega_m} \tag{3}$$

where ω_u and ω_l are the upper and lower frequency boundaries of the bandgap, respectively.

3.3.3 Final PnC Design

The Shamrock shaped phononic crystals were chosen for the waveguide design due to their superiority shown in the bandgap simulation results in Section 4.2. The main objective of the bandgap of the PnC is to match it with the excited acoustic wave frequencies. Integration tests could not definitely prove that the mask designs create strong enough SAWs for the testing of the acoustic beam splitters. However, results indicate that there is a correlation between the pump laser spot size and the excited frequency. (See Section 4.1.2). For the determination of the bandgap of the PnC it had to be estimated what the expected frequencies will be of the acoustic waves in the waveguide. Looking at the tunability test in Section 4.1.2, frequencies around 0.1-0.3 GHz have been detected that possibly correlate to the spot size of the pump laser. Also, interference patterns were created that could possibly allow the tuning of the excited acoustic waves, if the power is large enough.

Still, there is uncertainty on how well acoustic wave excitation can be tuned by the setup. Therefore it was decided to create a range of PnCs and waveguides with different parameters. This approach increases the chance of success in matching the PnC bandgap with the excited acoustic wave. For determining the range of frequencies that could in theory be excited with the setup on a gold coated Si3N4 membrane, the following assumptions were made:

1. The speed of sound in the waveguide could vary between 2000-6000 m/s. Such a range was chosen to cover both the expected gold and Si3N4 SAW wave speeds separately.

2. The wavelength of the excited acoustic wave could vary between 3-15 um.

With the above range of wavelengths and acoustic wave speeds the expected frequencies can be calculated with the following relationship:

$$f = \frac{v}{\lambda} \tag{4}$$

where f is the frequency, λ is the wavelength and v is the speed of sound. The above considerations lead to the expected acoustic wave excitation frequencies in a range of:

$$0.13\ GHz < f_{expected} < 2\ GHz \tag{5}$$

To cover this large range of frequency spectrum with bandgaps, seven shamrock-type PnCs were designed. The design parameters and geometry of the lattice is shown in 23a and Table 1. To design for different bandgaps, the lattice constant a was varied to align the one PnC's upper bandgap limit to another PnC's lower bandgap limit. All of the PnCs are made of Si3N4 and have a membrane thickness of 200 nm and a pre-tension of 1 GPa.

3.4 Waveguide and splitter designs

The manufactured waveguides and splitters are made of high-stress 200nm thick Si3N4 suspended membranes coated with gold. Five variations of waveguides are made that are shown in Figure 24 and include the following features:

1. Straight waveguides are created to be able to test the exciting, guiding and detecting of acoustic waves on a simplified structure. Results from these simple waveguide can also serve as reference/comparison to results of more complex structures (splitters, interferometers). See Figure 24a.
2. Splitters are created to be able to demonstrate the guiding and splitting of acoustic waves within the structure. There are two versions of splitters : "hard" and "soft" splitter. Soft splitters are surrounded by the PnC all around, while hard splitters have empty space between the two split arms. See Figure 24 b and c.
3. "Interferometers" are created to be able to test how split acoustic waves interfere when they are guided into each other. These structures are essentially the combination of two mirrored beam splitters attached together. Soft and hard interferometers are made. For hard interferometers, material is removed between the two waveguide arms. See Figure 24 d and e.

All structures use the earlier discussed Shamrock-type phononic crystals explained in Section 3.3.3. To create the wide range of bandgap needed, designs with seven different lattice constant variations are created that result.

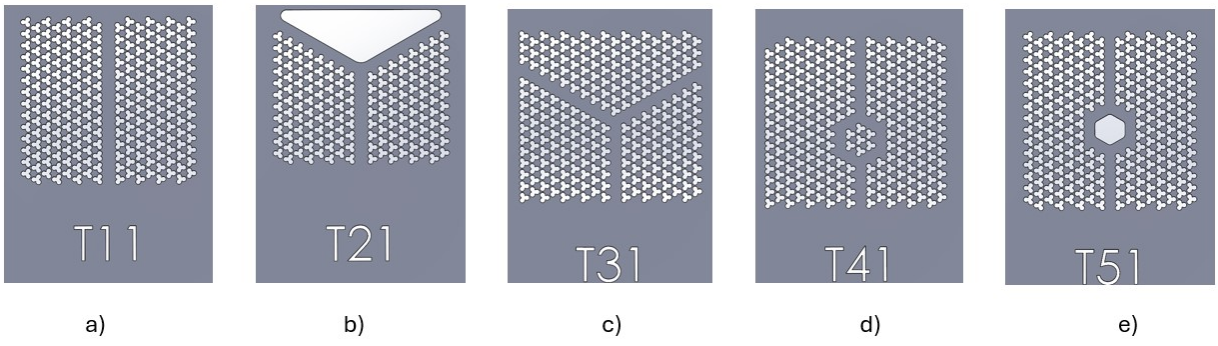

Figure 24: The 5 types of waveguides: a) Simple straight wave guide b) Hard beam splitter c) Soft beam splitter d) Soft interferometer e) Hard interferometer

The final chip layout is shown in Figure 25. Each box includes the designs with a given lattice constant. Each row within a box is a different type of waveguide, splitter or interferometer. Each column is a scaled version

(by 1%) of the neighboring structure. As can be seen from the Figure, for smaller lattice constants there are more rows within a box. This is because on these structures also several waveguide width were made. The spot size of the laser is about 8um: for a 1.5um lattice constant this would be very large and so the waveguide width had to be scaled as well. The expectation is that a thin waveguide that is smaller than the laser spot, will still detect the acoustic signals within the waveguide.

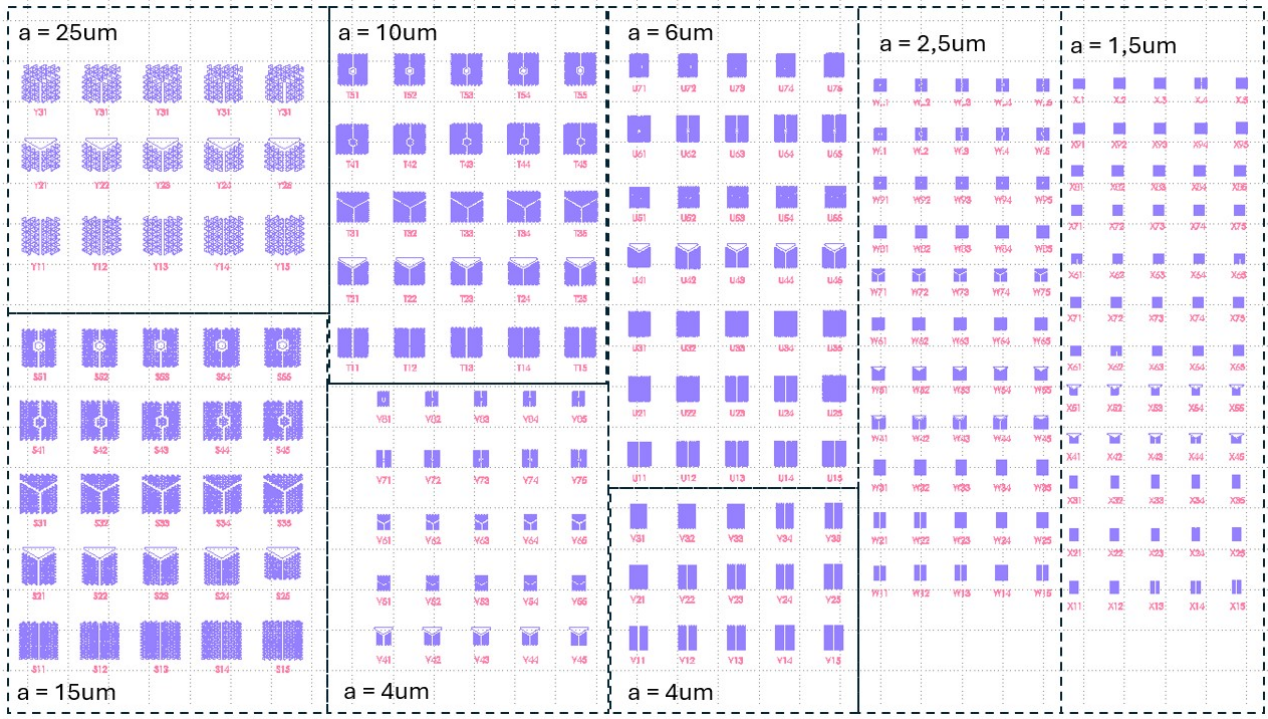

Figure 25: Mask design of the different acoustic waveguides, beam splitters and interferometers. Each box in the figure shows the relevant PnC lattice constant (letter a). Note that the lattice constant is varied in each column by 1% per column within a box.

4 Results

4.1 Integration tests

In this section the results of the tests described in Section 3.2 are presented. These tests were done to learn more about the setup and the sample before the final designs of the acoustic beam splitters are made. The following question needed to be investigated that are presented in this section:

1. Setup capabilities for SAW excitation and measurement: in what frequency range is the setup capable of exciting and measuring GHz SAW's and over what wave travel distances?
2. Tunability: Is it possible to tune the excited SAW frequencies to match them with the bandgap of the PnC?
3. Material: how do different materials used as a coating enhance signal strength?

4.1.1 Setup capabilities for SAW excitation and measurement

Figure 26 shows a measurement for when the pump and probe spots are focused on the same spot on the gold coated SiN membrane. A strong 0.2 GHz mode is present, alongside some weaker modes, alongside a fast 26 GHz mode. The 26GHz mode is only present in the first third of the temporal signal (from about 0.3 to 3 ns) after which it has decayed so much that it is not detectable. This mode is a BAW that is echoing back and forth between the top and bottom surface of the gold layer in the membrane. The travel time of one echo is 0.038 ns (1/26GHz) and the speed of sound in gold (for a BAW) is around 3250 m/s. Therefore, the travel distance of one back and forth echo is 0.038*3250 = 124 nm . This would mean that the thickness of the gold layer should be 62 nm, which is in good agreement of the expected gold layer thickness (40-70nm). The 2 GHz mode and higher modes indicated with green arrows are likely an artifact of the measurement equipment, as these modes are visible in all measurements, even with the pump laser off.

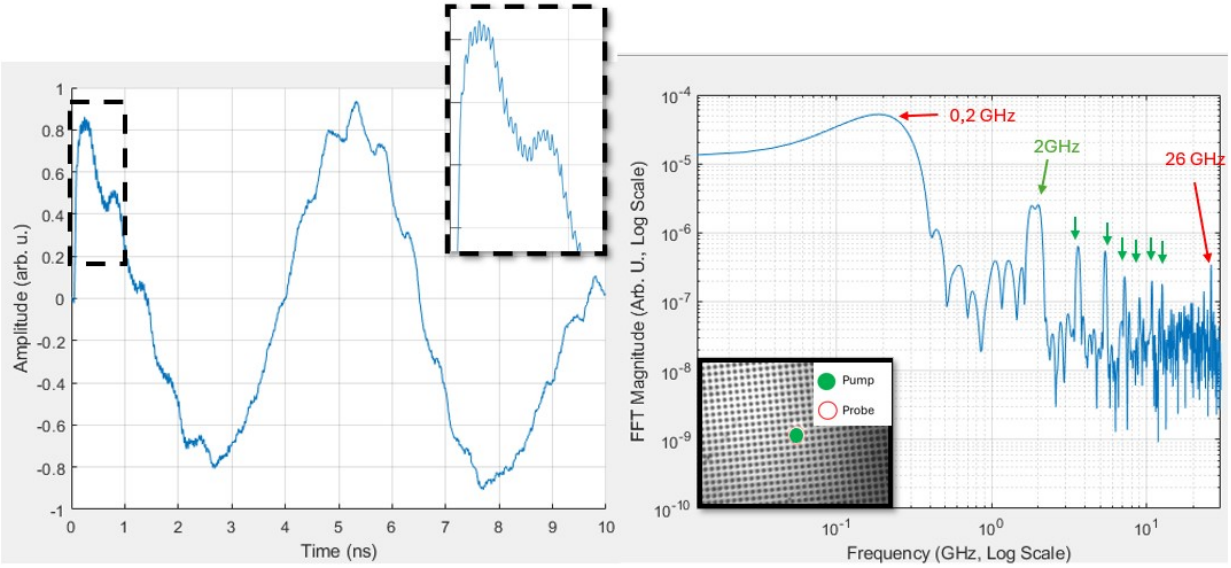

Figure 26: a) Signal on a Au coated SiN membrane. The location of excitation and probing is coincident b) FFT of the measured signal in log scale. A strong peak is observed at 0.2 GHz. This mode is also clearly visible in the time domain signal (large amplitude vibration). The 26 GHz mode (see dashed inset) is the result of BAW waves bouncing back and forth in the "bulk" of the membrane. Green arrows indicate the harmonics of the 2GHz mode that is most likely an artifact of the measurement. setup. Inset: an image of the sample showing the conicident location of both the pump and probe laser spots. Dashed insert: zoom-in on the 26GHz time domain signal.

Long traveling SAW and Lamb waves?

Two dominant acoustic modes have been identified across the membrane: a 0.3GHz mode and a far reaching 0.1GHz mode. Figure 27 shows the 0.3GHz mode measured at a distance of 16 μm between pump and probe spots. This mode is typically observed in the near-, and midfield signals. If we assume, this mode has a wavelength equal to the spot size of the pump (and probe) laser of around $8\mu m$, the resulting speed of this acoustic wave would be around:

$$v = 8e^{-6}m * 0.3e^{9}1/s = 2400m/s \tag{6}$$

This speed is close to the expected SAW velocity in an gold thin film[33]. It is therefore plausible, that the 0.3GHz mode is a SAW with its wavelength determined by the spot size of the pump laser.

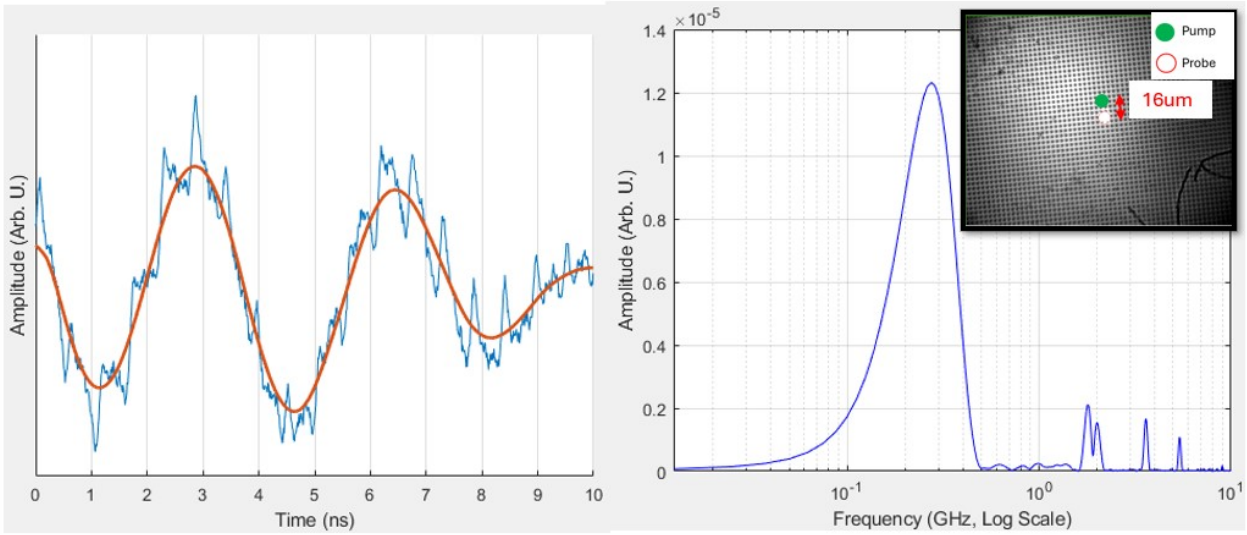

Figure 27: a) Time domain signal of a measurement with 16um distance between pump and probe spots. A a high-pass filter (200Mhz) is applied to hide a high amplitude 0.1 GHz mode that will be discussed later. b) FFT of the signal. A 0.3 GHz mode is present in the acoustic signal. Red line is a low pass filtered signal to highlight the 0.3GHz mode. Note that in this example the peak is not exactly at 0.3GHz. It is rounded off because of the relatively low frequency resolution of the FFT and the slight variation of the mode's frequency across different measurements.

Figure 28 shows the 0.3 GHz mode for several measurements at varying distances. A high-pass (200MHz) and low-pass(600MHz) filter were applied to the temporal acoustic signal to create these plots. The phase velocity of this mode was calculated by assuming that the peaks depicted by the black arrows are indeed the "same" peaks arriving at a later time due to the larger distance they travel. For example, considering the purple and green curves in the plot:

$$v = \frac{49 - 40}{7.2 - 3.2}\frac{\mu m}{ns} = 2250m/s$$

Calculating the average speed of all the peaks combined yields:

$$v_{avg} = 2650m/s \tag{7}$$

This value is not much above the velocity determined earlier in Equation 6, further supporting the theory, that the 0.3GHz mode is indeed a SAW traveling in the gold layer. In Figure 28a it is also clearly visible how the amplitude of this SAW decays with distance. This amplitude decay is further discussed later in Figure 30b.

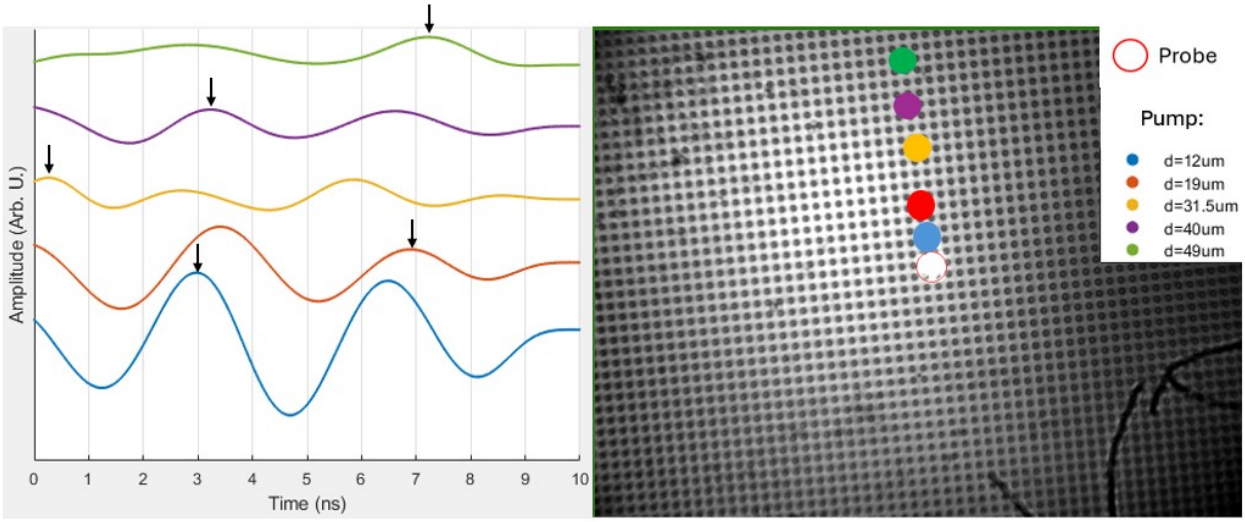

a) b)

Figure 28: Evolution of the signal for increasing distance between pump and probe spots. The signal is filtered with a high-pass(200MHz) and low-pass(400Mhz) filter to isolate the roughly 0.3 GHz mode described earlier. a) Time domain amplitude of the isolated 0.3 GHz mode for varying distances. To estimate the phase velocity of this mode, the peaks depicted with black arrows were assumed to be the same peaks, arriving at a later time due to the extra distance they had to travel. Calculating the speed of the phase based on this presented data, an average speed of 2650 m/s is found, that is comparable to the expected speed of a SAW in gold coating depositid on Silicon [33]. b) Image of the membrane depicting excitation and probe locations. Inset shows the exact values of distance.

The 0.1 GHz wave for various distances is shown in Figure 29. At these far-field measurements it is the only dominant acoustic mode present in the signal: the 0.3 GHz wave fades away in the far-field. Similarly to the 0.3 mode, here a phase shift was observed with growing distance: see the arrows in the figure. The phase shift in this case is negative, which is at first glance surprising: with growing distance it is expected that the phase arrive later in the time delay plot due to the extra distance it has to travel. This seeming contradiction can be explained with the phase having a very low velocity. With a slightly larger distance to travel, the phase does not arrive **earlier**, as suggested by the Figure 29, but actually almost 10 ns **later**, in the "next 10 ns slot". Due to the ASOPS method applied by the measurement setup, there is no way to distinguish between the two scenarios. For example, returning to Figure 29, the peak of the yellow curve at 8 ns could actually have a time delay of 8ns, 18ns, ...or 8+m*10ns, where t=0 is the moment the pump hits the sample and m is an integer.

So, assuming that in Figure 29a the phase shift is explained by a low phase velocity of the mode, the speed of the wave can be calculated: by dividing the distance difference between two measured by the negative phase time delay plus 10 ns. For example, to calculate the phase velocity between the yellow and purple curves in Figure 29a

$$v = \frac{d}{t} = \frac{66 - 60um}{8.8 - 9.5 + 10ns} = 645m/s \tag{8}$$

This speed suggests that the 0.1 GHz acoustic wave is an Antisymmetric Lamb wave mode (A0), as it nicely fits the phase velocity dispersion relations for a 200nm thick Si3N4 plate calculated in Appendix A.3.

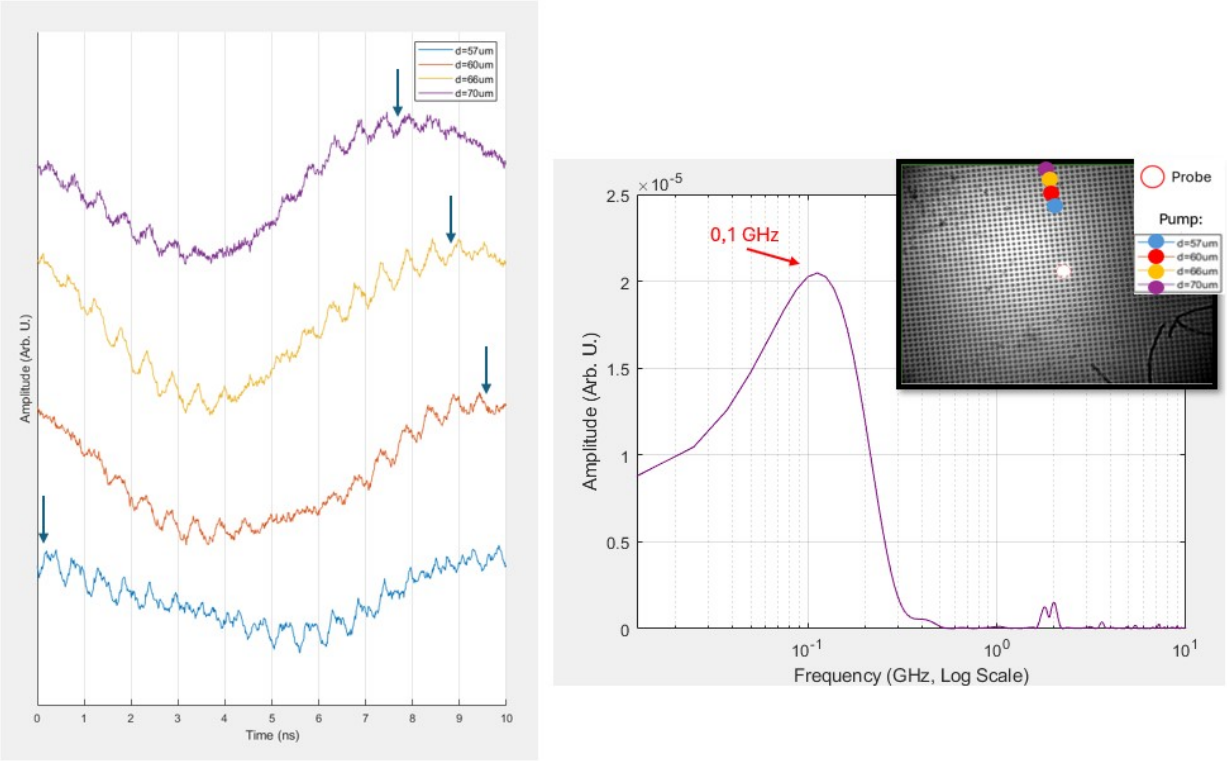

Figure 29: a) Time domain signals of measurements at varying distances. A large amplitude 0.1 GHZ mode is present. The small amplitude vibrations (at 2GHz in the FFT) are an artifact of the measurement setup. A clear negative shift with growing distance (see black arrows) suggest that this is a slow a traveling wave, likely an antisymmetric Lamb A0 mode. b) FFT of the signal at 70um showing a high peak around 0.1 GHz. The inset shows the image of the gold coated membrane with the pump and probe spot locations for each measurement.

Amplitude decay of the 0.1 and 0.3 GHz acoustic waves

The amplitude at each measured distance has been plotted of the 0.1 and 0.3 GHz acoustic waves in Figure 30. A curve is fitted over the measurement results. Note, that for a 2D acoustic wave spreading from a point source, the wave amplitude is inversely proportional to the square root of the distance to the point source:

$$A \propto \frac{1}{\sqrt{r}} \tag{9}$$

where A is the amplitude of the wave and r is the distance to the point source.

Because both reflectometry and BDD measurement signals are directly proportional to the acoustic wave amplitude[16], the relation between the amplitude of signal and the distance between probe and pump spots are expected to hold the same relation as stated in Equation 9. As can be seen from the figure, there is good agreement between such a fitted curve and the measurement results. This result further suggests, that the 0.1 and 0.3 GHz modes are both traveling waves, spreading from a point source (pump laser spot).

Fluctuations are present in the measurement data compared to the fitted curve. This can be caused by several factors: due to the hole patterns, the membrane is an-isotropic. Therefore, acoustic waves do not exactly spread in a circular pattern. Also, between measurements the setup had to often be fine-tuned making the sensitivity of the setup never exactly the same for each measurement.

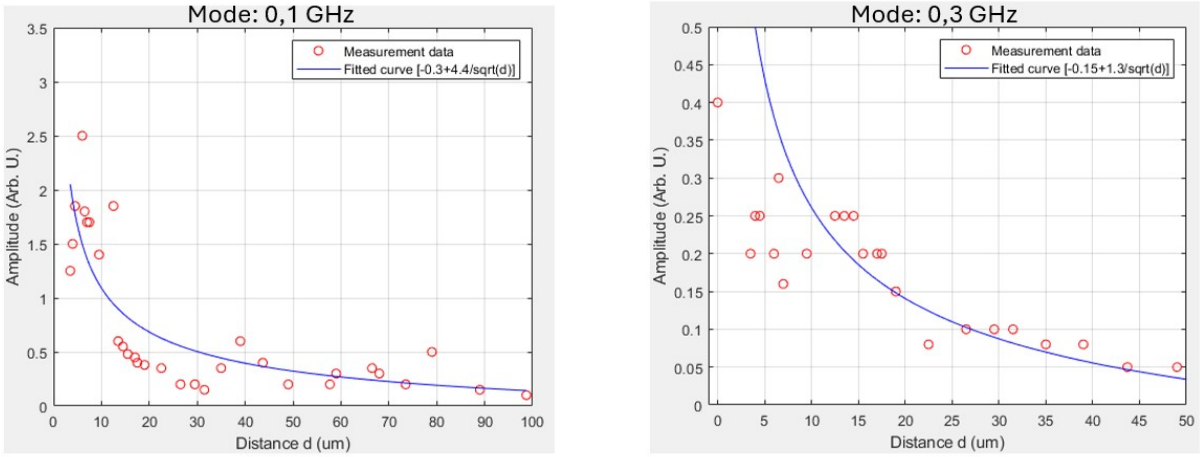

Figure 30: Amplitude of the measured acoustic signals as a function of the distance between pump and probe spots. A curve is fitted to show proportionality between amplitude, and the inverse of the square root of the distance. a) Amplitude vs Distance plot for the 0.1 GHz mode. b) Amplitude vs Distance plot for the 0.3GHz mode

4.1.2 Tunability experiments: interference pattern and spot size manipulation

This section presents the results of the experiments outlined Section 3.2.2. Two methods are explored that potentially allow the excitation of tunable SAWs with the fs laser reflectometry pump-probe setup:

1. Interference pattern creation on the sample surface with the use of masks in the pump beam.
2. Shifting the focus of the laser to enlarge/shrink the pump laser spot size.

1. Interference pattern creation on the sample surface with the use of masks

Tests have confirmed that the masks described in Section 3.1.2 indeed create interference patterns on the sample and that the distance between the patterns indeed changes with the different mask geometries, see Figure 31.

Tests were done with the probe laser because its lower wavelength is more detectable with the camera. During the test, images were made of the interference patterns and their fringe spacing was determined. Figure 31b shows the results. Tightly packed dark and light fringes can be observed that vary almost linearly with the aperture distance d on the mask. This test has confirmed that easily tunable interference patterns can be created with this setup using a fast fs pulse laser. Literature has shown (Section 2.5) that such interference patterns result in SAWs in the sample with a wavelength equal to the fringe spacing.

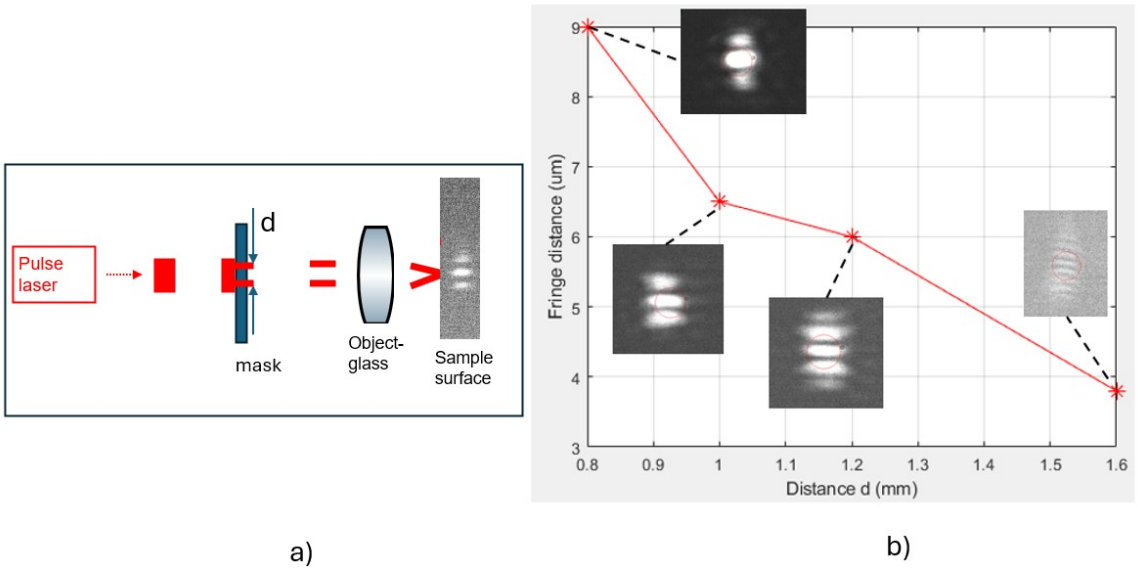

Figure 31: a) Schematic of the working principle of the masks as described in Section 3.2.2. These tests were done with the probe laser (780nm). Distance d was varied between 0.8mm and 1.6mm. The aperture diameters were kept constant at 0.6mm. b)Fringe distance spacing of the interference patterns observed on the sample surface versus Distance d between the apertures on the mask. See insets of the images taken during the experiment. It is observed that the fringe spacing is indeed dependent on the distance d between the apertures on the mask.

Measurements were done on the gold coated membranes using these masks to excite acoustic waves. A typical signal is shown in Figure 32a. Probe and pump lasers were aligned for this measurement. It was observed that although there is still an acoustic signal, the signal-to-noise ratio has significantly been reduced due to the mask. This is because a large portion of the laser power is blocked by the mask and therefore never reaches the sample. In Appendix A.2 it is estimated that masks used in these measurement roughly block $90 - 98\%$ of the original laser power, depending of the exact geometry of the mask. In Figure 32b the FFT is shown after passing the signal through a high-pass filter. The expected SAW frequency is shown with orange shaded area. This area was applied as a bandwidth filter to the time delay signal, see the inset on Figure 32b. With the filter applied, a decaying 0.6 GHz mode is made visible that is likely caused by the interference pattern. However, because of the high noise this could not be definitely verified. Note, that the sample is covered with holes, causing even more laser power not reaching the sample surface. In the final waveguide design, the laser excitation surface will be continuous, and so it remains to be seen if this mask design with this laser setup can create and tune SAWs efficiently.

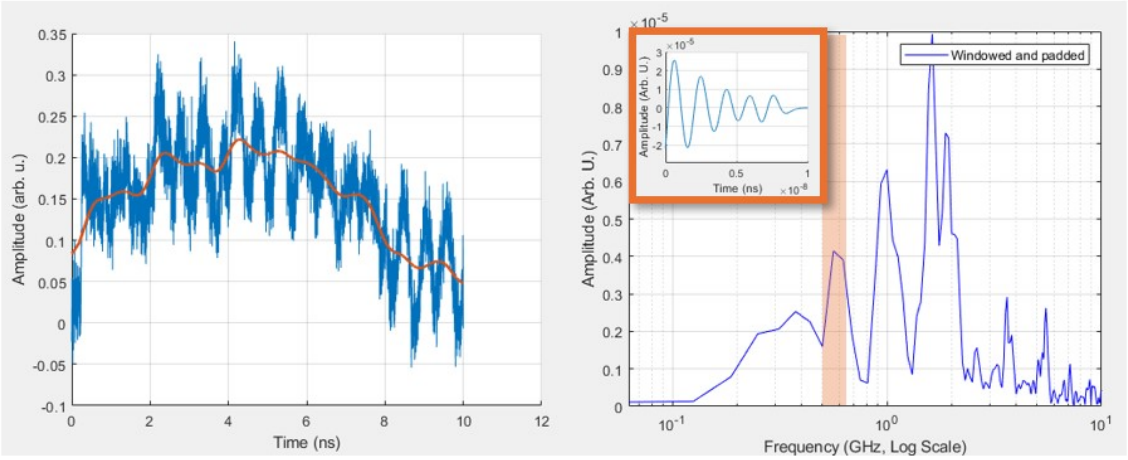

Figure 32: a) Acoustic signal of the gold coated membrane with a mask placed in the path of the pump pulse laser. There is still an acoustic signal, but the signal-to-noise ratio has dropped significantly compared to measurements where no mask is used, due to the drop of laser power reaching the sample. b) FFT of the time domain signal, after applying a high pass filter (200MHz). The orange shaded are is where the expected SAW should be present for the used interference pattern (wavelength = 4-5.5um). Inset with orange border shows the time domain signal with an applied filter of a bandwidth given by the orange shaded area. There is a 0.6 GHz mode present in the signal. This is likely an acoustic mode, because of the consistently decaying amplitude. However, because of the low signal-to-noise ratio, this can not be considered hard evidence for the working of the mask.

2. Spot size variation of the pump (and probe) laser spot

Figure 33b shows the results of several measurements for different laser spot sizes. The laser spot size was changed be shifting the membrane sample around the focus of the objective. A mode was detected that shifted in its frequency with the spot diameter and which approximately satisfied the assumption that the spot size is about equal to the wavelength of the excited SAW (yellow curve in Figure 33b. These results suggest that there is indeed a correlation between a frequency component of the acoustic wave and the laser spot size it is excited with. As can be seen in the figure, for larger spot sizes the excited frequencies tend to be lower, which is to be expected and also have been seen in literature[28]. Figure 33a shows a measurement for spotsize 14 um and frequency component of 250MHz. The red data point is measured on a different, larger membrane. Since the measured surface is covered with holes, significant variation could be expected in the results depending on how well the pump probe illuminates the actual sample surface.

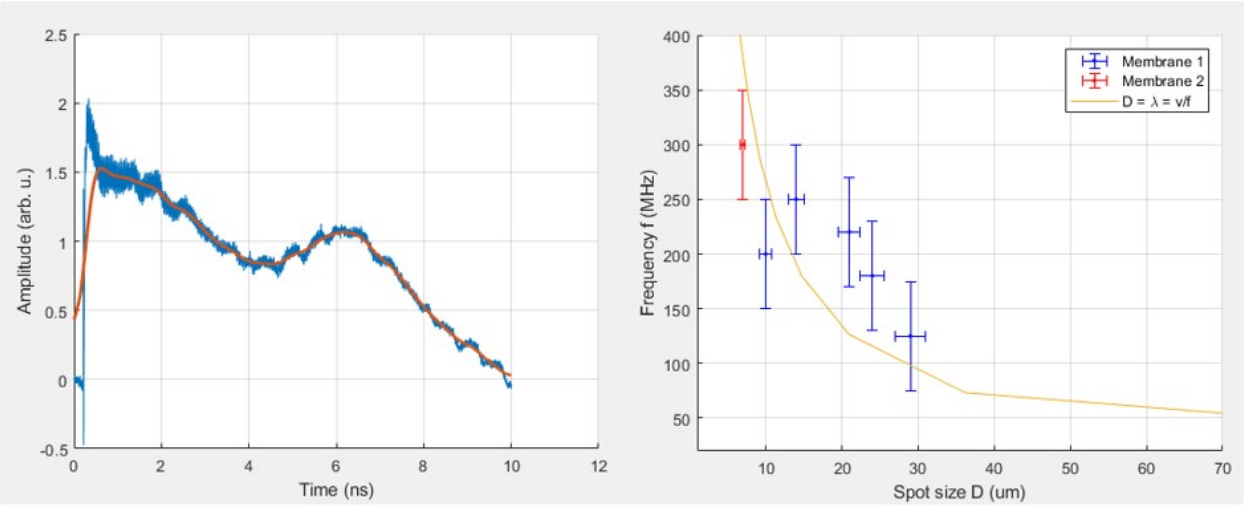

Figure 33: a) Acoustic wave signal measured for a spot diameter of 14um with a mode of 250 MHz c) Measured Frequency vs laser spot diameter. The red data point is measured on another, larger membrane compared to the blue stars. Error bars are added to the spot size and frequency. There seems to be a correlation between the spot size and an acoustic mode(0.15-0.3GHz), as expected from literature[28]. The yellow curve is the calculated spot diameter based on the earlier determined speed of SAW in the membrane (Equation 7) and assuming D = wavelength(λ). The experimental data follows the growing trend of the theoretical curve, however, there is variation in offset present. This could be due to the fact that the membrane is covered in holes and therefore a varying portion of the pump spot does not reach the membrane. Also, for large spot sizes the signal-to-noise ratio decreases significantly due to both the pump and probe spots being out of focus, thereby decreasing both excitation and detection laser power per unit area.

4.1.3 Material experiments

Typical measurement results for the NbTiN and Au coatings are shown in Figure 34. As can be seen from in the figure, the signal on gold is significantly better. The thermal peak is a factor 2 higher, but more importantly, the acoustic response itself is at least an order of magnitude higher. It was also noticed during testing that the NbTiN coating sometimes got damaged during testing with the pump laser. The gold coating never experienced this issue. The damage on the NbTiN surface suggests that the coating can not absorb the laser pulses without ablation, thereby not being able to transfer optical energy into mechanical strain efficiently.

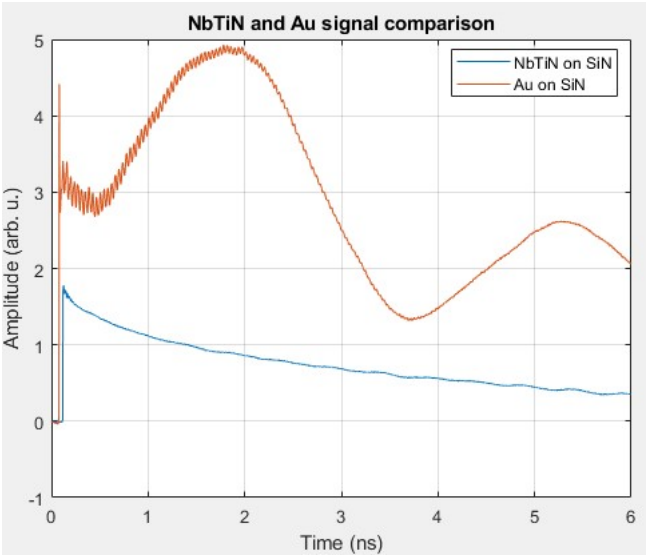

Figure 34: Signal strength comparison between SiN membranes coated with NbTiN and with Au (gold). In both cases the pump and probe spots were focused on the same spot. As can be seen from the figure, the gold coated sample shows strong acoustic BAW(26 GHz) and SAW(0.3 GHz) modes, orders of magnitude higher than the NbTiN coating. This could simply be caused by the ablation of the NbTiN coating experienced due to the high laser power. However, this result could also suggest that NbTiN is less efficient in converting infrared laser light into mechanical strain due to its different thermal properties compared to gold, for example its lower thermal conductivity or absorption.

4.2 Phononic Crystal Designs

This section present the design of the phononic crystals that will be used for the final acoustic waveguide designs. The method of how these simulation and design results were obtained are outlined in Section 3.3

4.2.1 PnC Lattice Comparison

Figure 35 shows the band diagrams of the shamrock and circle shaped hexagonal PnCs described in Section 3.3.2. The Gap-to-Midgap ratios have been determined to be 36% and 8%, respectively. It is evident from the simulation results that the shamrock shaped lattice structure provides a relatively large bandgap, confirming the results presented by Florez et al. [12]. The large bandgap in the shamrock design can be explained by the mass distribution of the material within a unit cell: larger mass centers connected by thin tethers[12]. Based on these simulation results the decision was made to use shamrock shaped holes in the acoustic waveguide. A wide bandgap will increase the chance that the excited acoustic frequency falls within the bandgap.

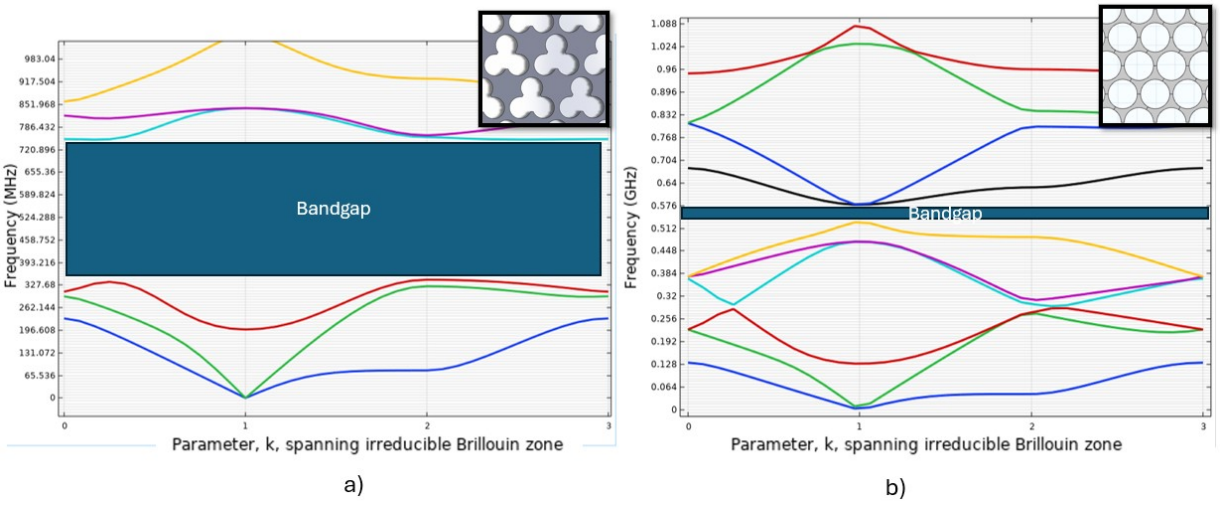

Figure 35: a) Band diagram of the Shamrock shaped PnC lattice with a Gap-to-Midgap ratio of 36%. Inset shows the shamrock lattice structure. b) Band diagram of the circle patterned PnC lattice with a Gap-to-Midgap ratio of 8%. Inset shows the circle lattice structure. The lattice parameters for both PnCs are described in Section 3.3.2

4.2.2 Final PnC design

As described in Section 3.3.3, seven different PnCs were designed by varying their lattice constant a. The plots for each of the band diagrams can be found in Appendix A, together with the geometrical parameters of each lattice. Figure 36a shows the Shamrock type lattice used for the design, Figure 36b shows the range of the bandgaps as a function of the lattice constant used for the beam splitter designs. As can be seen from the plot, the size of the bandgap scales inversely with the the lattice constant: for larger lattice constants the bandgap becomes narrower.

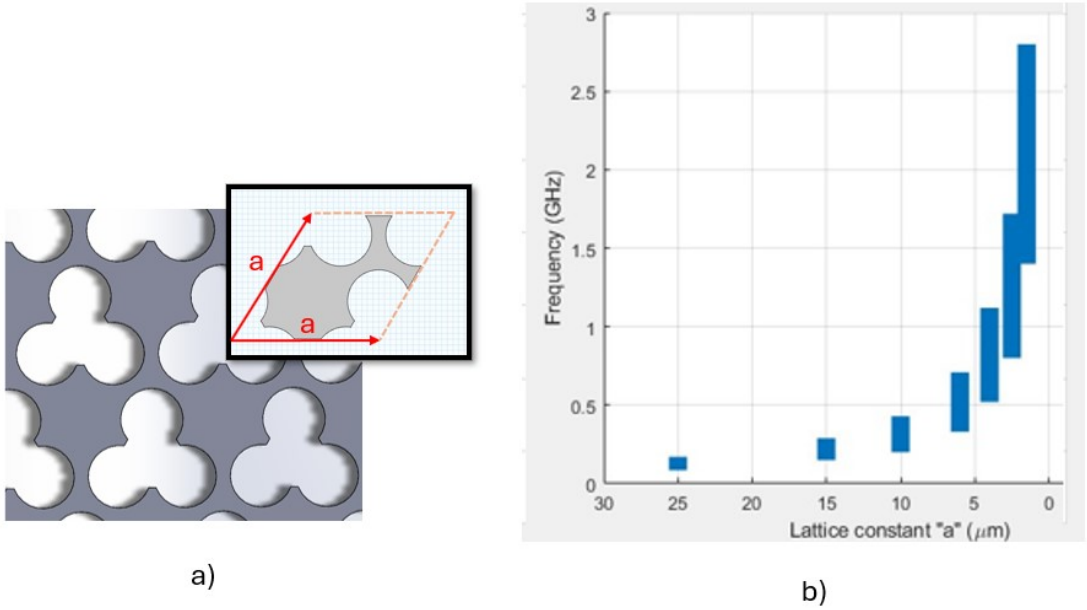

Figure 36: a) Shamrock type PnC lattice with lattice constant a b) Bandgap of the different PnCs as a function of their lattice constants. In total, a bandgap frequency range from 0.08 to 2.6 GHz is covered with the combination of these crystals. These different PnCs allow for experimentally determining which lattice constant works best with the laser setup.

4.3 Acoustic waveguide and splitter designs

The designed acoustic wavguides, splitters and interferometers presented in Section 3.4 have been manufacture. The 200nm thick Si3N4 membranes are covered with a 20 nm gold coating.

Images of some of the waveguides are shown in Figure 37. A total of 255 devices have been designed and manufactured, that incorporate the different PnC bandgap ranges described in Section 4.2.2. While most of the devices were released successfully, this is not true for some of the larger lattice constant devices. As can be seen in Figure 37g, some areas of the interferometer device is not suspended.

Due to delay in manufacturing and time constraints, the rigorous testing of these many waveguides could not be preformed during this thesis project, unfortunately. However, some tests have been performed where successful guiding and splitting of acoustic waves are demonstrated. This is presented in the following section.

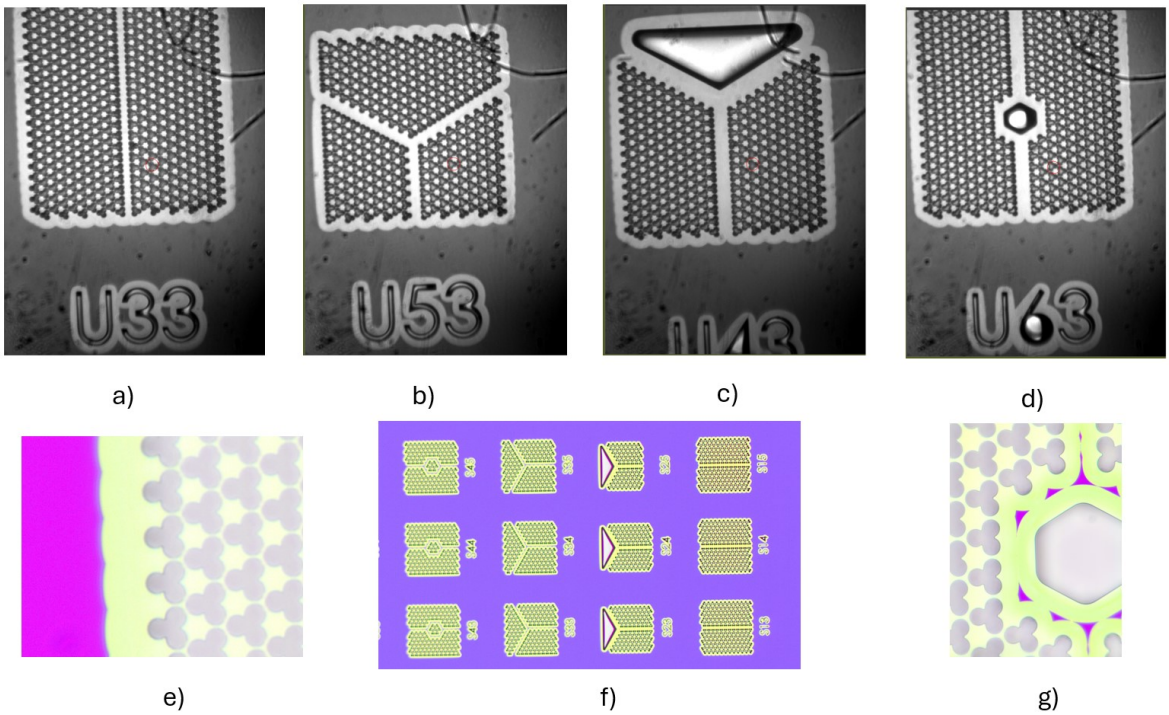

Figure 37: Manufactured waveguides based on Shmarock-type hexagonal PnC lattices. a) straight waveguide b) Soft-splitter c) hard-splitter d) interferometer e) Zoom-in on the Shamrock-type PnC structure used in the designs f) Zoom-out image of several devices next to each other g) Zoom-in image of a device where the waveguide is not fully suspended (purple areas in the center). In total 255 different devices have been made, with varying parameters of their incorporated PnC bandgaps as described in Section 4.2.2.

4.4 Splitting of guided acoustic waves

Qualitative tests were performed on the acoustic beam splitters with lattice constants $a = 15\mu m$ and $a = 6\mu m$ and bandgaps centered around 200 MHz and 540MHz, respectively. See the calculated bandgaps of these crystals in Appendix A. The goal of these measurement was to:

1. Demonstrate that the setup is capable of exciting and measuring acoustic waves on the waveguides to then guide and split them in two separate directions.
2. Show that the PnC indeed possesses a bandgap at approximately the designed/simulated range (see Section 4.2.2).

In the measurements shown in Figure 38 the pump is located on the straight part of the device, while the probe is placed either on the left or right arm of the splitter. The PnC of the device has a lattice constant $a = 15\mu m$ and a theoretical bandgap of $f_b = 150 - 280MHz$. Measurements clearly show the presence of a strong 0.1 and a weak 0.3 GHz mode, similar to the measurements on the simple suspended membranes (Section 4.1.1). The question then arises if these modes are truly confined to the waveguide, or are they present across the whole suspended structure. This can be checked by placing the probe spot on the PnC lattice. This is done in Figure 39a. It can be seen that the 0.1 GHz mode is not present in the crystal at the measured location, showing that the mode is at least partially blocked by the PnC and confined to the waveguide. The same measurement is repeated on another PnC, where the bandgap is much higher ($f_b = 350 - 700MHz$), see Figure 39b. It can be seen, that on that PnC, the 0.1 GHz mode is present in the crystal. These results are a promising indication that the devices can confine, guide and split GHz acoustic waves on compact suspended SiN structures at the expected frequencies.

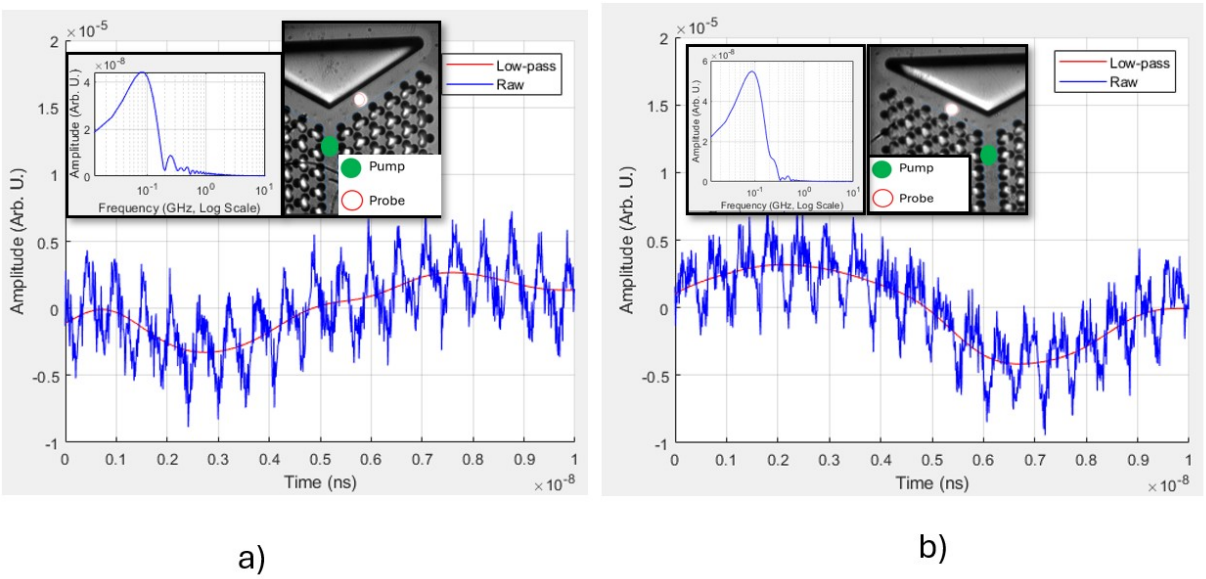

Figure 38: Acoustic signals on beam splitters with PnC lattice constant $a = 15\mu m$ and a theoretical bandgap of $f_b = 150 - 280MHz$. The pump laser (green spot) is placed on the straight waveguide, while probing (white spot with red edge) occurs on the right (a) and left (b) arm of the splitters. Insets show the position of the laser pulses, and the FFT of the low-pass (500MHz) filtered signal, respectively. The blue signal is the raw time delay data, the red curve is the low-pass filtered signal (at 500MHz), to exclude high frequency system interference and noise components not related to the acoustic signal. In both arms the 0.1 GHz and 0.3 GHz modes are present that have already been examined earlier. To prove that these traveling waves are indeed confined to-, and split by the beam splitter, it was measured whether these modes are present in the crystal lattice, see Figure 39a. As can be seen in the Figure, little to no such modes are detected in the crystal lattice. Note, that the detected 0.1GHz mode does not fall in the theoretical bandgap of the PnC, but it is relatively near to it. This could be due to manufacturing tolerances and/or simulation inaccuracies. Further measurements should determine the exact range of the bandgap.

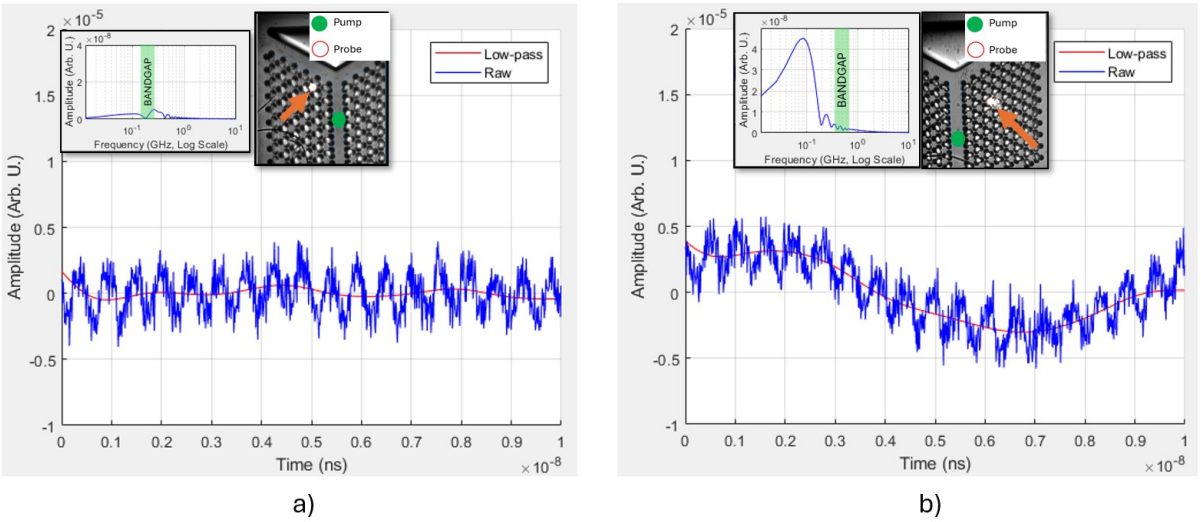

Figure 39: Acoustic signals excited on the straight waveguide section of the splitter (green spot) and measured on the PnC lattice (orange arrows). The distance and orientation of the probe and pump spots are kept the same as in Figure 38. a) Measurement on the same device as in Figure 38 with PnC lattice constant $a = 15\mu m$ and a bandgap centered around 200 MHz. b) Measurement on a device with lattice constant $a = 6\mu m$ and a theoretical bandgap centered around 540 MHz. Insets show the position of the laser pulses, and the FFT of the low-pass (500MHz) filtered signal, respectively. The bandgaps are depicted with green shaded areas in the FFT plots. As can be seen, the 0.1 GHz mode is barely present in the left plot, meaning that the mode is mostly confined to the waveguide (see Figure 38). In the right plot, the mode is present in the PnC, likely due to the PnC having a significantly higher bandgap (>0.35 GHz).

5 Discussion and Conclusion

In this thesis report:

1. Two approaches are presented and tested for the excitation of tunable SAWs with a femtosecond pump-probe reflectivity laser setup, offering an alternative excitation method not yet presented for such a setup in literature. Succesful tuning is achieved in the 0.1-0.3 GHz range. See Section 4.1.2.
2. Integration tests have been performed on a femtosecond reflectivity/BDD pump-probe setup to examine its capability in exciting and detecting acoustic waves at larger distances on suspended SiN membranes. See Section 4.1.1
3. New suspended Si3N4 acoustic waveguides and wave splitters have been designed and manufactured to study the capability of efficiently guiding and splitting GHz acoustic waves, see Section 4.3.
4. Qualitative measurement are performed to show the functionality of the designed beam splitters in guiding and splitting incoming acoustic waves. See Section 4.4.

5.1 Tunability of SAWs with an fs laser pump-probe setup

Two methods were tested in this thesis project to excite tunable SAWs on a SiN membrane with a femtosecond pump-probe reflectivity laser: laser spot size variation and interference pattern creation. The results are discussed in this section.

5.1.1 Laser Spot size vs. acoustic frequency

During experiments on gold coated SiN membranes, in Section 4.1 a correlation was found between the frequency of a SAW mode (0.3 GHz) and the pump laser spot size, as expected from literature[28]. This gave the motivation to tune the SAW frequency by simply shifting the focus of the pump laser around the surface to shrink or increase the diameter of the spot size, and thereby effecting the resulting SAW frequency. Figure 33 shows the results of this experiment. Results showed that this simple method changed the SAW frequency in a range from 125 to 300 MHz.

Downside of this technique is that enlarging the pump spot generates less heat difference, because the constant laser energy is spread out on a larger surface. This smaller heat difference results in weaker acoustic waves. Furthermore, the probing signal also weakens, because its diameter also gets enlarged.

Another disadvantage of this technique for an acoustic waveguide is that a simple Gaussian laser spot does not define the direction of the generated SAW: the SAW will propagate in a circular pattern, spreading the wave energy equally in all directions. For acoustic waveguides it would be preferred to excite plane waves in the direction of the waveguide only. This can be achieved by the interference pattern method discussed in the following section.

5.1.2 Interference pattern generation and SAW excitation with the use of masks

The presented and tested masks (Section 4.1.2) create repetitive dark and light laser interference fringes on the sample surface. In literature (Section 2.5) it has been proven that such a pattern excites SAWs with a defined frequency and direction.

The patterns were achieved by the use of masks that were placed in the path of the pump beam. The design allows for easy swap of the masks. Different masks, with different aperture geometries allow for easy manipulation of the interference pattern at the sample surface, thereby allowing for the tunability and direction of the excited SAWs. See results in Figure 31 for the different interference patterns.

The presented mask concept offers an easy solution for creating tunable interference patterns (i.e. SAWs) in a femtosecond reflectometry pump-probe setup, that has not yet been demonstrated in literature (see Section 2.4)

The downside of this design is that it significantly drops the pump laser power that reaches the sample surface: above 90% of the original laser power is not transmitted for most mask designs. This drop in signal strength results in a reduced signal-to-noise ratio. Measurements showed signs of tuned acoustic waves of around 0.6 GHz, however the high noise of the signal did not allow to definitely verify these results.

A possible solution for the above described SAW tunability issues could be to implement a spatial light modulator (SLM) in the setup. Such a device would allow agile interference pattern generation and manipulation, in combination with lower laser power losses.

5.2 Exciting and detecting GHz acoustic waves across a suspended SiN membrane with a fs pump-probe setup

Experiments were done with a femtosecond laser pump-probe setup to excite and detect SAWs on a suspended SiN membrane. The results are presented in this section.

5.2.1 SAW and Lamb waves

The measurement setup's capabilities for SAW excitation at different distances on a gold coated SiN membrane were tested, see results in Section 4.1.1. Even at a distance of $100\mu m$ from the excitation point, acoustic signals were successfully detected, raising confidence in the setup's capability to test the acoustic waveguides and beam splitters. A 0.3GHz mode was found to be a SAW caused by the spot size of the pump laser, bound to the gold layer of the membrane. A slow traveling Lamb acoustic mode at 0.1 GHz has also been identified that was detectable even at large distances of $100\mu m$ from the pump source. The amplitude decay with travel distance of the 0.1GHz (Lamb) and 0.3GHz(SAW) modes were plotted to find that their amplitude decays as expected for a wave spreading circularly from a point source, see (Figure 30).

These results show that the setup is sensitive enough to excite (near GHz) acoustic waves and detect them on a SiN membrane, allowing for the testing of the presented acoustic waveguides.

5.2.2 "BAW" in gold coating

"Bulk Acoustic Waves" were detected, with a frequency of around 26 GHz, related to the gold coating on the SiN membranes. "BAW" is in parentheses, since the thin gold coating can hardly be considered as bulk material. In Figure 26 a 26GHz mode is clearly visible in both the frequency and time domain signal. As discussed earlier in Section 4.1.1, this acoustic mode is a wave echoing back-and-forth between the top and bottom surface of the 60 nm thick gold coating.

5.3 Guiding and splitting of acoustic waves on a suspended SiN beam splitter

Gold coated SiN acoustic waveguides and beam splitter designs are manufactured and presented in this thesis project with the objective to demonstrate (for the first time[15]), the controlled splitting of acoustic beams on a suspended SiN PnC waveguide. Using COMSOL simulations, Shamrock-type hexagonal PnC lattice structures were designed to cover a bandgap ranging from 0.1 GHz to 3 GHz. These PnCs were used to build different types of acoustic waveguides, splitters and other structures. Due to time limitations, extensive testing of the 255 devices was not executed, this will hopefully be done soon by another researcher.

However, qualitative experiments were executed that show promising capabilities of selectively guiding and manipulating/splitting GHz acoustic waves on a suspended SiN membrane.

5.3.1 Recommendations and Outlook on the quantitative characterization of the acoustic waveguides

For the precise characterization of the waveguide and splitter designs, the setup could be upgraded with a spatial light modulator that allows precise control and higher signal-to-noise ratio of the excited acoustic waves. Once this control is available, the following experiments could be conducted to characterize the devices:

1. To characterize the splitting of the incoming acoustic waves, precise measurements of the amplitude changes in the splitter arms need to be measured. For this, sensitivity of the measurement setup needs to be consistently set.
2. Meanwhile, the bandgaps of the different PnCs could be characterized by sweeping the excitation frequencies. This would determine the bandwidth of the waveguides.
3. Measurements on the PnC crystals could be performed at different distances and frequencies to determine to what depth a mode within the bandgap penetrates the crystal from the waveguide.
4. Distance measurements on the waveguides and splitters could be performed to quantify how efficient the devices are in transporting the acoustic energy over longer distances.

A Appendix

A.1 PnC band diagrams and parameters

In this appendix are the bandgap simulation results for the different shamrock shaped PnCs, with their corresponding lattice constant and other parameters.

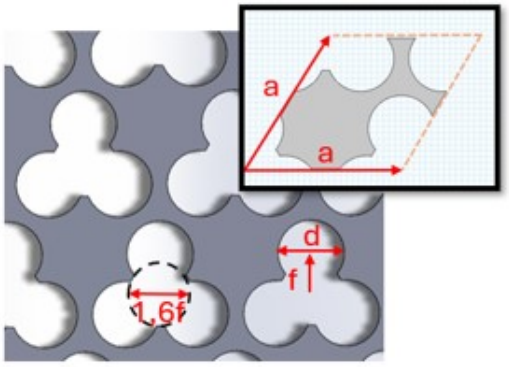

a)

a (um)	f (um)	d (um)
1,5	0,4	0,33
2,5	0,67	0,55
4	1,07	0,88
6	1,60	1,32
10	2,67	2,20
15	4,00	3,30
25	6,67	5,50

b)

Figure 40: a) Shamrock type PnC lattice used for the final design. b) The seven different sized lattice parameters that together cover the desired bandgap range

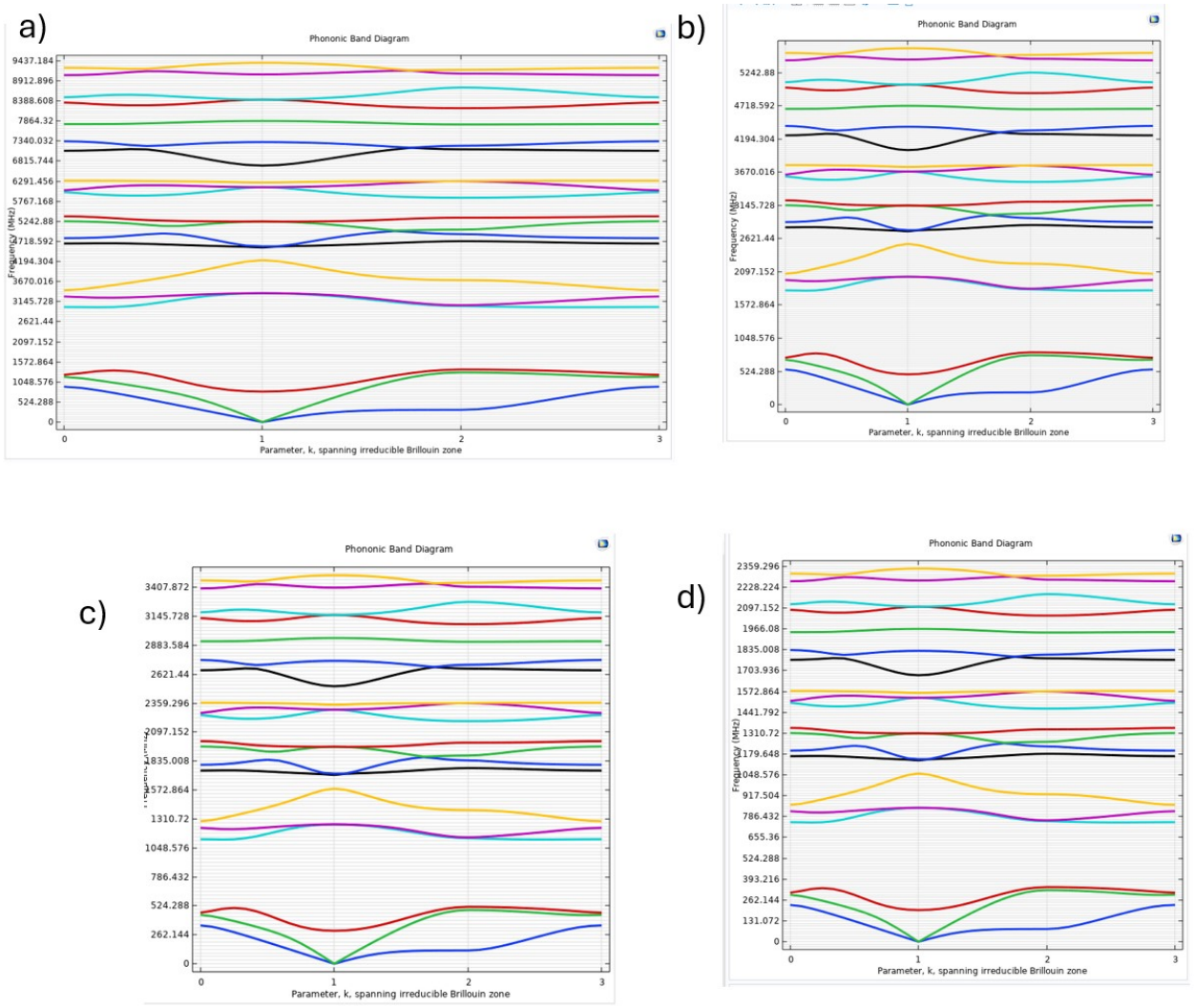

Figure 41: Band diagrams for Shamrock-patterened PnCs with lattice constants: a) 1.5um, b) 2.5um, c) 4um, d) 6um.

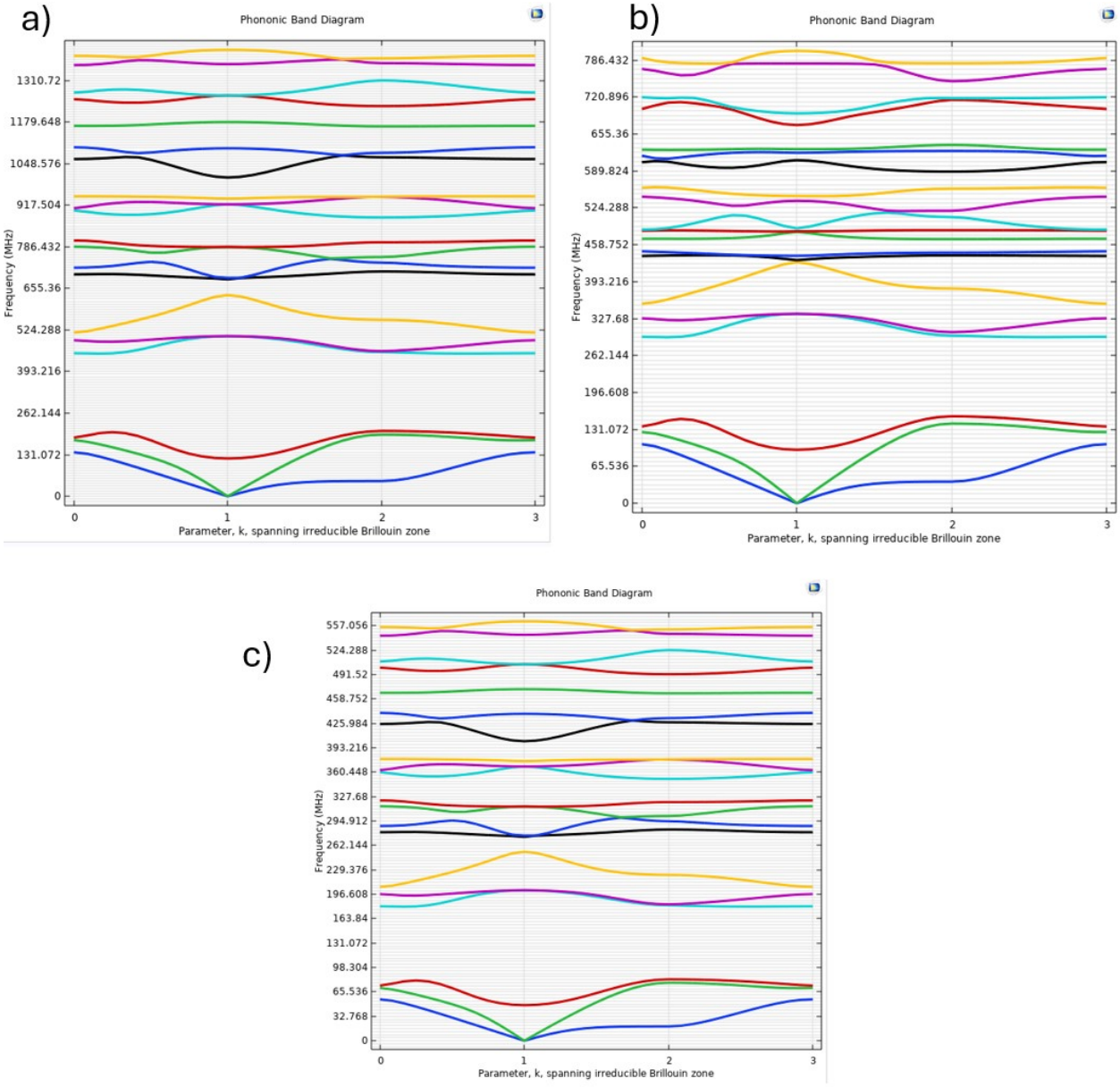

Figure 42: Band diagrams for Shamrock-patterened PnCs with lattice constants: a) 10um, b) 15um, c) 25um

A.2 Laser Power Loss Estimation with Mask

In this appendix it is estimated how much laser power is lost when the masks are used to create an interference pattern.

First, the power transmitted through a circular aperture of radius r aligned with the optical axis and with the Gaussian beam is calculated. The cumulative power transmitted is given by the equation[34]:

$$P(r) = P(\infty)\left[1 - \exp\left(-\frac{2r^2}{w_0^2}\right)\right] \tag{10}$$

where:

- $P(r)$ is the power transmitted through an aperture of radius r.
- $P(\infty)$ is the total power of the Gaussian beam (i.e., the power when the aperture radius is effectively infinite).
- w_0 is the beam waist.

For a beam waist $w_0 = 5mm$ and a a radius $0.5mm < r < 1mm$ the above equation yields a power transmission of $2\% < P_t < 7.5\%$ depending on the aperture radius.

Note that there are two apertures in the mask, which should increase the total power transmittance, however they are not centered to the peak intensity of the Gaussian distribution.

It is therefore safe to assume, that for most mask types, at least 90% of the initial pump laser power is blocked by the mask, if not more.

A.3 Phase Velocity Dispersion of a SiN membrane

In this appendix the dispersion relations are shown for Si3N4 and Au membranes. The relations are calculated using an MIT Licensed python code [35] that uses Lamb's characteristic equations to numerically solve the phase velocities of symmetric and anti-symmetric Lamb modes. As can be seen in Figure 43, the expected phase velocity of the A0 Lamb mode in a 200 nm thick Si3N4 plate is approximately 590 m/s.

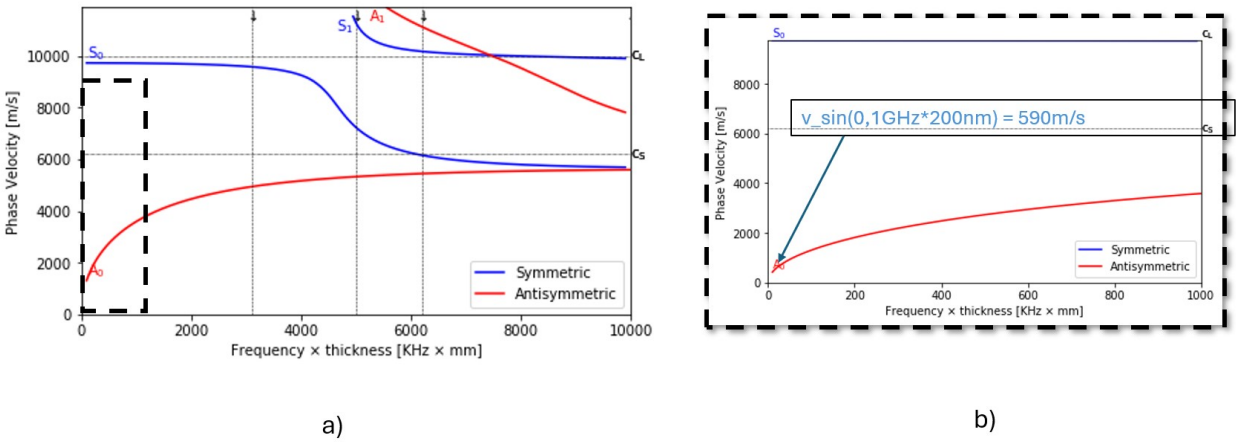

Figure 43: Phase velocity dispersion in a 200 nm thick Si3N4 plate. For a 200 nm thick plate and a 0.1 GHz A0 mode, calculations show a phase velocity of 591 m/s. The plot was made inputting a longitudinal wave velocity $c_L = 10000m/s$ and shear wave velocity $c_S = 6200m/s$ a) and b) represent the same results, with plot b) zoomed in on the x axis. These calculations were done with an MIT licensed code [35].

A.4 FFT calculations in Matlab

```
function analyze_full_fft(Sig,treal)

Fs = 1 / mean(diff(treal));       % Sampling frequency
T = 1/Fs;         % Sampling period
L = length(treal);

Y = fft(Sig);
P2 = abs(Y/L);
P1_raw = P2(1:L/2+1);
P1_raw(2:end-1) = 2*P1_raw(2:end-1);

f_raw = Fs/L*(0:(L/2));

% FFT processing
N = length(Sig); % Original length of the signal
N_fft = 8192; % New length for the FFT, typically a power of 2

%Zero pad the signal
Sig_p = [Sig; zeros(N_fft-N, 1)];

% Apply a window function to the signal
windowed_signal = Sig.* hamming(length(Sig));
%window the zero padded signal
windowed_padded_signal = Sig_p.* hamming(length(Sig_p));


% Zero-pad the windowed signal
Sig_wp= [windowed_signal; zeros(N_fft-N, 1)];

%Compute fft
Sig_wp_fft = fft(Sig_wp);
Sig_p_fft = fft(Sig_p);
Sig_w_fft = fft(windowed_signal);
Sig_pw_fft = fft(windowed_padded_signal);



% Sampling frequency
Fs = 1 / mean(diff(treal)); % Calculate based on time differences

% Spectrum analysis padded and windowed signal
P2wp = abs(Sig_wp_fft / N_fft);
P1wp = P2wp(1:N_fft/2+1);
P1wp(2:end-1) = 2*P1wp(2:end-1);
% Spectrum analysis padded and windowed signal
P2pw = abs(Sig_pw_fft / N_fft);
P1pw = P2pw(1:N_fft/2+1);
P1pw(2:end-1) = 2*P1pw(2:end-1);
% Spectrum analysis padded signal
P2p = abs(Sig_p_fft / N_fft);
P1p= P2p(1:N_fft/2+1);
P1p(2:end-1) = 2*P1p(2:end-1);
% Spectrum analysis windowed signal
P2w = abs(Sig_w_fft / N);
P1w= P2w(1:N/2+1);
P1w(2:end-1) = 2*P1w(2:end-1);
% Spectrum analysis windowed signal
P2w = abs(Sig_w_fft / N);
P1w= P2w(1:N/2+1);
P1w(2:end-1) = 2*P1w(2:end-1);
% Frequency vector
f = (Fs*(0:(N_fft/2))/N_fft)/10^9;
fw = (Fs*(0:(N/2))/N)/10^9;

%Plot the amplitude spectrum with peaks
figure();
plot(f, P1wp,"b",'DisplayName', "Windowed and padded");
% hold on;
% plot(f, P1pw,"b",'DisplayName', "Padded and windowed");
xlabel('Frequency (GHz, Log Scale)');
ylabel('Amplitude (Arb. U.)');
xlim([0,10]);
```

```
legend();
set(gca, 'XScale', 'log');  % Set the x-axis to logarithmic scale
grid on;

%Plot the amplitude spectrum with peaks
figure();
plot(f, P1pw,"b",'DisplayName', "Padded and windowed");
xlabel('Frequency (GHz, Log Scale)');
ylabel('Amplitude (Arb. U.)');
xlim([0,10]);
legend();
set(gca, 'XScale', 'log');  % Set the x-axis to logarithmic scale
grid on;

figure();
plot(f,P1p,"b",'DisplayName', "Zero-Padded FFT");
xlabel('Frequency (GHz, Log Scale)');
ylabel('Amplitude (Arb. U.)');
xlim([0,10]);
grid on;
set(gca, 'XScale', 'log');  % Set the x-axis to logarithmic scale
legend();

figure();
plot(f_raw*10^-9,P1_raw,'DisplayName', "Raw");
xlabel('Frequency (GHz, Log Scale)');
ylabel('Amplitude (Arb. U.)');
xlim([0,10]);
grid on;
set(gca, 'XScale', 'log');  % Set the x-axis to logarithmic scale
legend();

end
```

References

[1] Debdyuti Mandal and Sourav Banerjee. Surface acoustic wave (saw) sensors: Physics, materials, and applications. *Sensors*, 22(3), 2022.

[2] Ken-ya Hashimoto. *Bulk Acoustic and Surface Acoustic Waves*, pages 1–23. Springer Berlin Heidelberg, Berlin, Heidelberg, 2000.

[3] D.P. Morgan. *Surface Acoustic Wave Filters: With Applications to Electronic Communications and Signal Processing*. Electronic communications. Academic Press, 2007.

[4] Kejie Fang, Matthew H. Matheny, Xingsheng Luan, and Oskar Painter. Optical transduction and routing of microwave phonons in cavity-optomechanical circuits. *Nature Photonics*, 10(7):489–496, 2016.

[5] Per Delsing, Andrew N. Cleland, Martin J.A. Schuetz, Johannes Knörzer, Géza Giedke, J. Ignacio Cirac, Kartik Srinivasan, Marcelo Wu, Krishna Coimbatore Balram, Christopher Baüerle, Tristan Meunier, Christopher J.B. Ford, Paulo V. Santos, Edgar Cerda-Méndez, Hailin Wang, Hubert J. Krenner, Emeline D.S. Nysten, Matthias Weiß, Geoff R. Nash, Laura Thevenard, Catherine Gourdon, Pauline Rovillain, Max Marangolo, Jean Yves Duquesne, Gerhard Fischerauer, Werner Ruile, Alexander Reiner, Ben Paschke, Dmytro Denysenko, Dirk Volkmer, Achim Wixforth, Henrik Bruus, Martin Wiklund, Julien Reboud, Jonathan M. Cooper, Yong Qing Fu, Manuel S. Brugger, Florian Rehfeldt, and Christoph Westerhausen. The 2019 surface acoustic waves roadmap. *Journal of Physics D: Applied Physics*, 52(35), 2019.

[6] Christopher J. B. Ford. Transporting and manipulating single electrons in surface-acoustic-wave minima. *physica status solidi (b)*, 254(3):1600658, 2017.

[7] Linbo Shao, Di Zhu, Marco Colangelo, Daehun Lee, Neil Sinclair, Yaowen Hu, Peter T. Rakich, Keji Lai, Karl K. Berggren, and Marko Lončar. Electrical control of surface acoustic waves. *Nature Electronics*, 5(6):348–355, 2022.

[8] D. Hatanaka, I. Mahboob, K. Onomitsu, and H. Yamaguchi. Phonon waveguides for electromechanical circuits. *Nature Nanotechnology*, 9(7):520–524, 2014.

[9] Guilhem Madiot, Ryan C. Ng, Guillermo Arregui, Omar Florez, Marcus Albrechtsen, Søren Stobbe, Pedro D. Garcia, and Clivia M. Sotomayor-Torres. Optomechanical generation of coherent GHz vibrations in a phononic waveguide. pages 1–13.

[10] Yanan Wang, Jaesung Lee, Xu Qian Zheng, Yong Xie, and Philip X.L. Feng. Hexagonal Boron Nitride Phononic Crystal Waveguides. *ACS Photonics*, 6(12):3225–3232, 2019.

[11] Rishi N. Patel, Zhaoyou Wang, Wentao Jiang, Christopher J. Sarabalis, Jeff T. Hill, and Amir H. Safavi-Naeini. Single-Mode Phononic Wire. *Physical Review Letters*, 121(4):40501, 2018.

[12] O. Florez, G. Arregui, M. Albrechtsen, R. C. Ng, J. Gomis-Bresco, S. Stobbe, C. M. Sotomayor-Torres, and P. D. García. Engineering nanoscale hypersonic phonon transport. *Nature Nanotechnology*, 17(9):947–951, 2022.

[13] Felix M. Mayor, Wentao Jiang, Christopher J. Sarabalis, Timothy P. McKenna, Jeremy D. Witmer, and Amir H. Safavi-Naeini. Gigahertz Phononic Integrated Circuits on Thin-Film Lithium Niobate on Sapphire. *Physical Review Applied*, 15(1):1, 2021.

[14] Ziyao Feng, Yang Liu, Xiang Xi, Lai Wang, and Xiankai Sun. Gigahertz Phononic Integrated Circuits Based on Overlay Slot Waveguides. *Physical Review Applied*, 19(6):1, 2023.

[15] Maximiliaan van der Vis. Designing a suspended sin ghz acoustic beam splitter for room temperature operation designing a suspended sin ghz acoustic beam splitter for room temperature operation. Master's thesis, Delft University of Technology, 2022.

[16] Martin Robin, Ruben Guis, Mustafa Umit Arabul, Zili Zhou, Nitesh Pandey, and Gerard J. Verbiest. Conoscopic interferometry for optimal acoustic pulse detection in ultrafast acoustics, 2022.

[17] Timothy M. F. Hirsch, Nicolas P. Mauranyapin, Erick Romero, Tina Jin, Glen Harris, Christopher G. Baker, and Warwick . P. Bowen. Directional emission in an on-chip acoustic waveguide. 1(c):1–6, 2023.

[18] Nicolas P. Mauranyapin, Erick Romero, Rachpon Kalra, Glen Harris, Christopher G. Baker, and Warwick P. Bowen. Tunneling of Transverse Acoustic Waves on a Silicon Chip. *Physical Review Applied*, 15(5):1, 2021.

[19] Arun Arjunan, Ahmad Baroutaji, and John Robinson. Advances in Acoustic Metamaterials. *Encyclopedia of Smart Materials*, pages 1–10, 2021.

[20] Chi Zhang, Qiang Liu, and Zhengbiao Ouyang. Band Gap Optimization for GHz Elastic Waves in Gold Phononic Crystals. *IOP Conference Series: Materials Science and Engineering*, 585(1), 2019.

[21] Xiaoqiang Sun, Xiangyan Ding, Feilong Li, Shijie Zhou, Yaolu Liu, Ning Hu, Zhongqing Su, Youxuan Zhao, Jun Zhang, and Mingxi Deng. Interaction of lamb wave modes with weak material nonlinearity: Generation of symmetric zero-frequency mode. *Sensors (Switzerland)*, 18(8):7–26, 2018.

[22] Wikipedia contributors. Seismic wave, 2023. Online accessed.

[23] B. Bonello, A. Ajinou, V. Richard, Ph. Djemia, and S. M. Chérif. Surface acoustic waves in the GHz range generated by periodically patterned metallic stripes illuminated by an ultrashort laser pulse. *The Journal of the Acoustical Society of America*, 110(4):1943–1949, 2001.

[24] Michael Colletta, Wanjiru Gachuhi, Samuel A. Gartenstein, Molly M. James, Erik A. Szwed, Brian C. Daly, Weili Cui, and George A. Antonelli. Picosecond ultrasonic study of surface acoustic waves on periodically patterned layered nanostructures. *Ultrasonics*, 87:126–132, 2018.

[25] A. A. Maznev and O. B. Wright. Optical generation of long-lived surface vibrations in a periodic microstructure. *Journal of Applied Physics*, 105(12), 2009.

[26] A Vega-Flick, J K Eliason, A A Maznev, A Khanolkar, M Abi Ghanem, N Boechler, and K A Nelson. Laser-induced transient grating setup with continuously tunable period. 123101(December 2015), 2018.

[27] Kenji Katayama, Hayato Inoue, Hisashi Sugiya, Qing Shen, Taro Toyoda, and Keith A Nelson. Generation and detection of tunable phonon polaritons using a single transmission grating. *Applied Physics Letters*, 92(3), 2008.

[28] C.M. Scala and Doyle. Time- and frequency-domain characteristics of laser-generated ultrasonic surface waves. *The Journal of the Acoustical Society of America*, 1569(1989), 1989.

[29] N. Chigarev, C. Rossignol, and B. Audoin. Surface displacement measured by beam distortion detection technique: Application to picosecond ultrasonics. *Review of Scientific Instruments*, 77(11), 2006.

[30] Joseph W. Goodman. *Introduction to Fourier Optics*. Roberts and Company Publishers, Englewood, CO, 3rd edition, 2005. Fourier Transforming Properties of Lenses.

[31] unkown. Lecture 18: The convolution theorem. MIT OpenCourseWare: 2.71 Optics, Spring 2009, 2009. Accessed: 2024-05-24.

[32] COMSOL. Modeling Phononic Band Gap Materials and Structures. https://www.comsol.com/blogs/modeling-phononic-band-gap-materials-and-structures/, 2023. [Accessed: insert-date-of-access-here].

[33] E. Salas, R. J. Jiménez Riobóo, C. Prieto, and A. G. Every. Surface acoustic wave velocity of gold films deposited on silicon substrates at different temperatures. *Journal of Applied Physics*, 110(2), 2011.

[34] CVI Melles Griot. Gaussian Beam Optics (Guia Técnico Online). (1):594–596, 2009.

[35] Francisco Rotea. Lamb-wave-dispersion. https://github.com/franciscorotea/Lamb-Wave-Dispersion, 2024. MIT License, Accessed: 2024-06-06.